DEVELOPMENT OF A TSUNAMI FORECAST MODEL FOR GARIBALDI, OREGON

Aurelio Mercado

November 2008

DRAFT

Contents

Abstract 9
1.0 Background and Objectives 9
2.0 Forecast Methodology 9
2.2.1 Data Assimilation and Inversion 10
2.2.2. Standby Inundation Model Forecasting 10
3.0 Model Setup 11
3.1 Study Area – context 11
2.2 Reference Grids 15
2.3 Forecast model grids 19
3.0 Results 26
3.1 Model Validation 26
3.1.1 Tonga May 2006 26
3.1.2 Kuril Nov 2006 30
3.2 Model Stability and Reliability 33
3.3 Results of Tested Events 34
4.0 Discussion 46
5.0 Summary and Conclusions 68
6.0 Acknowledgements 69
7.0 References 69
8.0 Appendix A 70
8.1 forecast model *.in file for Garibaldi, OR forecast model 70
8.1 RIM *.in file for Garibaldi, OR forecast model 71

DRAFT

List of Tables

Table 1 Garibaldi, Oregon 1/3" arc second DEM attributes.....15

Table 2 Reference grid metadata for Garibaldi, Oregon 18

Table 3 Forecast model grid parameters for Garibaldi. 21

Table 4 MOST Model set up parameters for Garibaldi, OR.....22

Table 5 Historical events used to validate the Garibaldi forecast model 25

Table 6 Artificial megatsunami sources uses for testing the Garibaldi, OR forecast model.....26

Table 7 Example *.in file for Reference runs.....67

Table 8 Example *.in file for forecast runs 67

DRAFT

List of Figures

Figure 1 Location of study site 12

Figure 2 Google view of Tillamook Bay showing the swampy area that was the cause of instabilities in the reference Grid C enclosed inside the white curve. 12

Figure 3 Google map of the site the Garibaldi area. 13

Figure 4 The figure shows the location of the tide gauge used as the Warning Point. 13

Figure 5 Contour plot of NGDC DEM for Garibaldi, OR 14

Figure 6 Contour plot of the reference Grid A. The outlines of the finally adopted reference Grids B and C are also shown. The black cross shows the location of the Warning Point. 16

Figure 7 Contour plot of reference Grid B, and the outline of reference Grid C. 17

Figure 8 Contour plot of Grid_C_ref_2-3rds_v11.dat. Land values are not color filled. Blue cross shows location of Warning Point. 17

Figure 9 Zoom of the bay entrance, showing the steep slopes inside it. 19

Figure 10 3-D view of bay entrance. 20

Figure 11 Outline of Reference grids (RIM) 23

Figure 12 Outline of forecast grids (forecast model) 24

Figure 13 Original time history for 2006 Tonga event. 28

Figure 14 Zoom of above figure.....28

Figure 15 Demeaned original series, spline fit, and tsunami signal.....29

DRAFT

Figure 16 Time history comparison. Blue curve is the RIM, red curve is the forecast model, and black curve is the observed event. 30

Figure 17 Original time history for 2006 Kuril event. 31

Figure 18 Zoom of tsunami event. 31

Figure 19 Zoom of above figure, showing the outliers (blue) and the "corrected" signal (black). 32

Figure 20 Demeaned original series, spline fit, and tsunami signal.....32

Figure 21 Time history comparison. Blue curve is the RIM, red curve is the forecast model, and black curve is the observed event. 33

Figure 22 Time series comparison RIM vs. forecast model for 1946 Unimak event. .34

Figure 23 Time series comparison RIM vs. forecast model for 1994 Kuril event. 35

Figure 24 Time series comparison RIM vs. forecast model for 1996 Andreanof event. 35

Figure 25 Time series comparison RIM vs. forecast model for the 2001 Peru event. 36

Figure 26 Time series comparison RIM vs. forecast model for the 2003 Rat Island event. 36

Figure 27 Time series comparison RIM vs. forecast model for 2006 Tonga event. ...37

Figure 28 Time series comparison RIM vs. forecast model for the 2006 Kuril event. 37

Figure 29 Time series comparison RIM vs. forecast model for the 2007 Kuril event. 38

Figure 30 Time series comparison RIM vs. forecast model for 2007 Solomon event. 38

Figure 31 Time series comparison RIM vs. forecast model for 2007 Peru event.....39

DRAFT

Figure 32 Time series comparison RIM vs. forecast model for the 2007 Chile event. 39

Figure 33 Maximum Envelope of Highest Water for the 1946 Unimak event. 41

Figure 34 Maximum Envelope of Highest Water for the 1994 Kuril event. 41

Figure 35 Maximum Envelope of Highest Water for the1996 Andreanof event. 42

Figure 36 Maximum Envelope of Highest Water for the 2001 Peru event. 42

Figure 37 Maximum Envelope of Highest Water for the 2003 Rat Island event.....43

Figure 38 Maximum Envelope of Highest Water for the 2006 Tonga event. 43

Figure 39 Maximum Envelope of Highest Water for the 2006 Kuril event. 44

Figure 40 Maximum Envelope of Highest Water for the 2007 Kuril event. 44

Figure 41 Maximum Envelope of Highest Water for 2007 Solomon event. 45

Figure 42 Maximum Envelope of Highest Water for the 2007 Peru. 45

Figure 43 Maximum Envelope of Highest Water for 2007 Chile event. 46

Figure 44 Attempt 1 for T01_1946Unimak_j1_weco. 47

Figure 45 Attempt 2 for T01_1946Unimak_j1_weco. 48

Figure 46 Attempt 3 for T01_1946Unimak_j1_weco. 48

Figure 47 Attempt 4 for T01_1946Unimak_j1_weco. 49

Figure 48 Attempt 5 for T01_1946Unimak_j1_weco. 50

Figure 49 Attempt_5 for T01_1946Unimak_j1_weco with comparison at location more to the middle of the entrance channel. 51

DRAFT

Figure 50 Attempt 6 for T01_1946Unimak_j1_weco. 51

Figure 51 Attempt_6 comparison at location more to the middle of the entrance channel. 52

Figure 52 Attempt 7 for T01_1946Unimak_j1_weco. 53

Figure 53 - Location mid-way in the entrance channel. 53

Figure 54 Location completely outside the entrance channel. 54

Figure 55 Attempt 8 for T01_1946Unimak_j1_weco. 54

Figure 56 Attempt 9 for T01_1946Unimak_j1_weco. 55

Figure 57 Attempt 10 for T01_1946Unimak_j1_weco. 56

Figure 58 Attempt 10 - Comparison outside of entrance channel. 56

Figure 59 Attempt 11 for T01_1946Unimak_j1_weco. 57

Figure 60 Time series results at a warning point location completely outside entrance channel. 58

Figure 61 Attempt 12 for T01_1946Unimak_j1_weco. 58

Figure 62 Attempt 13 for T01_1946Unimak_j1_weco. 59

Figure 63 Attempt 14 for T01_1946Unimak_j1_weco. 60

Figure 64 Attempt 15 for T01_1946Unimak_j1_weco. 61

Figure 65 Attempt 16 for T01_1946Unimak_j1_weco 61

Figure 66 Attempt 17 for T01_1946Unimak_j1_weco. 62

Figure 67 T01_1946Unimak_j1_weco – time history at 50 m isobath west of entrance to the channel. 64

DRAFT

Figure 68 T01_1946Unimak_j1_weco – time history inside bay just south of the city of Garibaldi 65

Figure 69 Time history comparison in which the "forecast" grid C has the same area coverage as the reference grid C, but a resolution of 2 s.....66

DRAFT

Development of a Tsunami Forecast Model for Garibaldi, Oregon

Aurelio Mercado

DRAFT

Abstract

This report describes the development of a tsunami forecast model for Garibaldi, Oregon as a component of the NOAA SIFT system. The optimized MOST model can obtain accurate amplitude of first waves and reasonable inundation limit within 10 minutes for the study area upon receiving the information of the earthquake source determined from real-time data assimilation and inversion. The model is validated using numerical results from historical tsunami instrumental records for the area. The developed forecast model is tested against different scenarios of large virtual tsunamis generated in the Pacific Ocean and found that

1.0 Background and Objectives

The NOAA Center for Tsunami Research at NOAA Pacific Marine Environmental Laboratory is developing a tsunami forecasting tool known as Short-term Inundation Forecasting for Tsunamis (SIFT) for NOAA Tsunami Warning Centers (Titov *et al.*, 2005). The primary goal of the system is to provide NOAA Tsunami Warning Centers with operational tools that combine real-time deep-ocean Bottom Pressure Recorder (BPR) recordings from the DART tsunameter network (González *et al.*, 2005) and seismic data with a suite of numerical codes, Method of Splitting Tsunami (MOST) (Titov and Synolakis, 1998; Titov and González, 1997), to produce efficient forecasts of tsunami arrival time, heights and inundation. To achieve accurate and detailed information on the likely impact of incoming tsunami on specific coastal communities within certain time limits and to reduce false alarms, tsunami forecast models are being developed and integrated as crucial components of SIFT for of 75 US coastal cities and territories that are potentially at most risk.

The primary objective of the present study is to develop and test a model for real-time forecast of tsunami waves and inundation for the city of Garibaldi, Oregon.

2.0 Forecast Methodology

2.1 Tsunami Model

MOST (Titov and Synolakis, 1998; Titov and González, 1997) is a 2D finite-differences numerical model based on the nonlinear long-wave approximation. It uses a splitting scheme to separate the original two-dimensional problem into two sequential one-dimensional problems.

The MOST model accommodates a base level grid (0), for wave transoceanic propagation and three levels of telescoping grids (A, B, and C) with increasing spatial and temporal resolution for simulation of wave inundation onto dry land. The linear solution is evaluated at the base level while the nonlinear are calculated at the next three. Grid 0 is not dynamically couple with the other three, which is more efficient since it can provide multiple sets of boundary conditions for subsequent detailed calculations at different locations.

The numerical solution is obtained by an explicit finite-differences scheme with a second-order approximation in space and first order in time. The MOST model uses a Neumann-type technique to determine the waterline position through the computed flow velocity.

DRAFT

2.2 Methodology for NOAA SIFT System

The PMEL real-time tsunami forecasting scheme is a process that comprises of two steps, (1) data assimilation and inversion, and (2) forecasting by tsunami forecast models. Each one of these two steps is explained next

2.2.1 Data Assimilation and Inversion

Besides seismic and coastal tide gauges, real-time deep ocean bottom pressure data from the Deep-ocean Assessment and Reporting of Tsunamis (DART) tsunameter network, is used as a primary data source since it can provide rapid tsunami observation without harbor and instrument responses. The linearity of wave dynamics of tsunami propagation in the deep ocean allows for applications of inversion schemes to construct a tsunami scenario based on the best fit to given tsunameter data. Details of the inversion method can be found in Titov *et al*. (2003) and Wei *et al*. (2003).

PMEL has developed a linear propagation model database for unit sources in the Atlantic and Caribbean Sea, with each unit source a typical Mw = 7.5 subduction zone earthquake. Based on a sensitivity study of far-field tsunami characteristics (Titov *et al*., 1999), the parameters of the unit sources are: length = 100 km, width = 50 km, dip = 15°, rake = 90°, depth = 5 km, slip = 1 m. The strike of each source is aligned with the local orientation of the subduction zone. The model simulation results for each unit solution, including amplitudes and velocities, are stored in a database. (Gica et al. 2008). The inversion algorithm, which combines real-time tsunami-meter data of offshore amplitude with the propagation database, provides an accurate offshore tsunami scenario without additional time-consuming model runs.

2.2.2. Standby Inundation Model Forecasting

The forecast model applies the non-linear components of the MOST model using three nested grids (A, B, and C), with increasing resolution to telescope into the inundation forecasting area. The inundation area (grid C) includes the high concentration of population in the coastal communities, and the National Weather Service warning points,

To provide site-specific forecasting for rapid, critical decision-making in emergency management, forecast model are implemented and optimized for both speed and accuracy. First, a forecast model utilizes the pre-computed time series of offshore wave height and depth-averaged velocity from the database as the boundary and initial conditions once the offshore scenario is defined. Second, by reducing the calculation areas and grid resolutions, the optimized setup can provide forecasting results within 10 minutes (for a minimum of 4 hours of simulation time), which allows larger time steps without violations of the CFL conditions. Finally, to insure forecasting accuracy, results from the optimized runs are validated with historical tsunami tide gauge records (if available) as well as a reference model run made with higher resolutions and larger calculation domains.

DRAFT

3.0 Model Setup

3.1 Study Area – context

Figure 1 shows the location of the study site, Garibaldi, OR. Figure 2 shows a zoom of Tillamook Bay, along whose north shore the city of Garibaldi is located. The inside the white polygon shown to the southeast of the bay lies a swampy region which was the source of several instabilities in the reference Grid C. Figure 3 shows the Google Maps view of the study area.

DRAFT

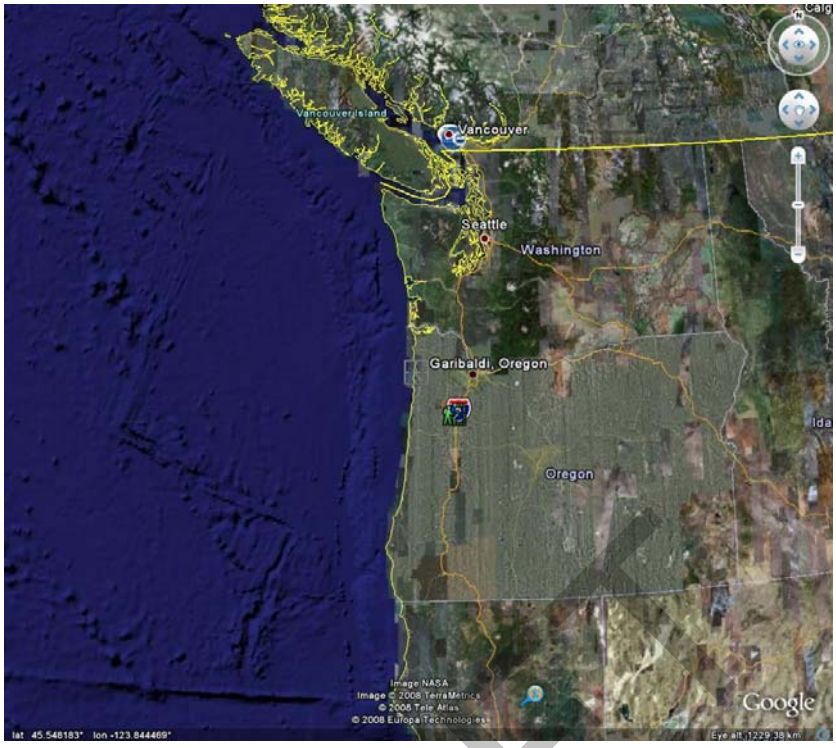

Figure 1 Location of study site

Figure 2 Google view of Tillamook Bay showing the swampy area that was the cause of instabilities in the reference Grid C enclosed inside the white curve.

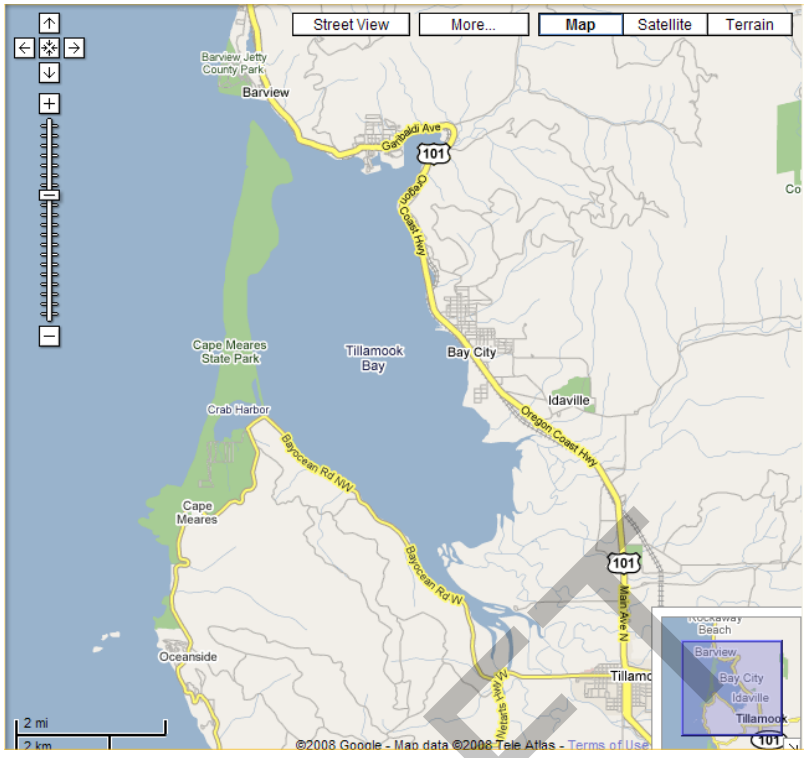

Figure 3 Google map of the site the Garibaldi area.

Figure 4 shows the location of the tide gauge which was adopted as the Warning Point.

Figure 4 The figure shows the location of the tide gauge used as the Warning Point.

The adopted location to obtain the time histories was -123.943009° W, 45.5667° N.

A filled contour plot of the Garibaldi, Oregon DEM is shown in Figure 5. This will serve as the bathymetry and topography source for the reference and optimized Grids B and C. Table 2-2 shows the DEM metadata.

DRAFT

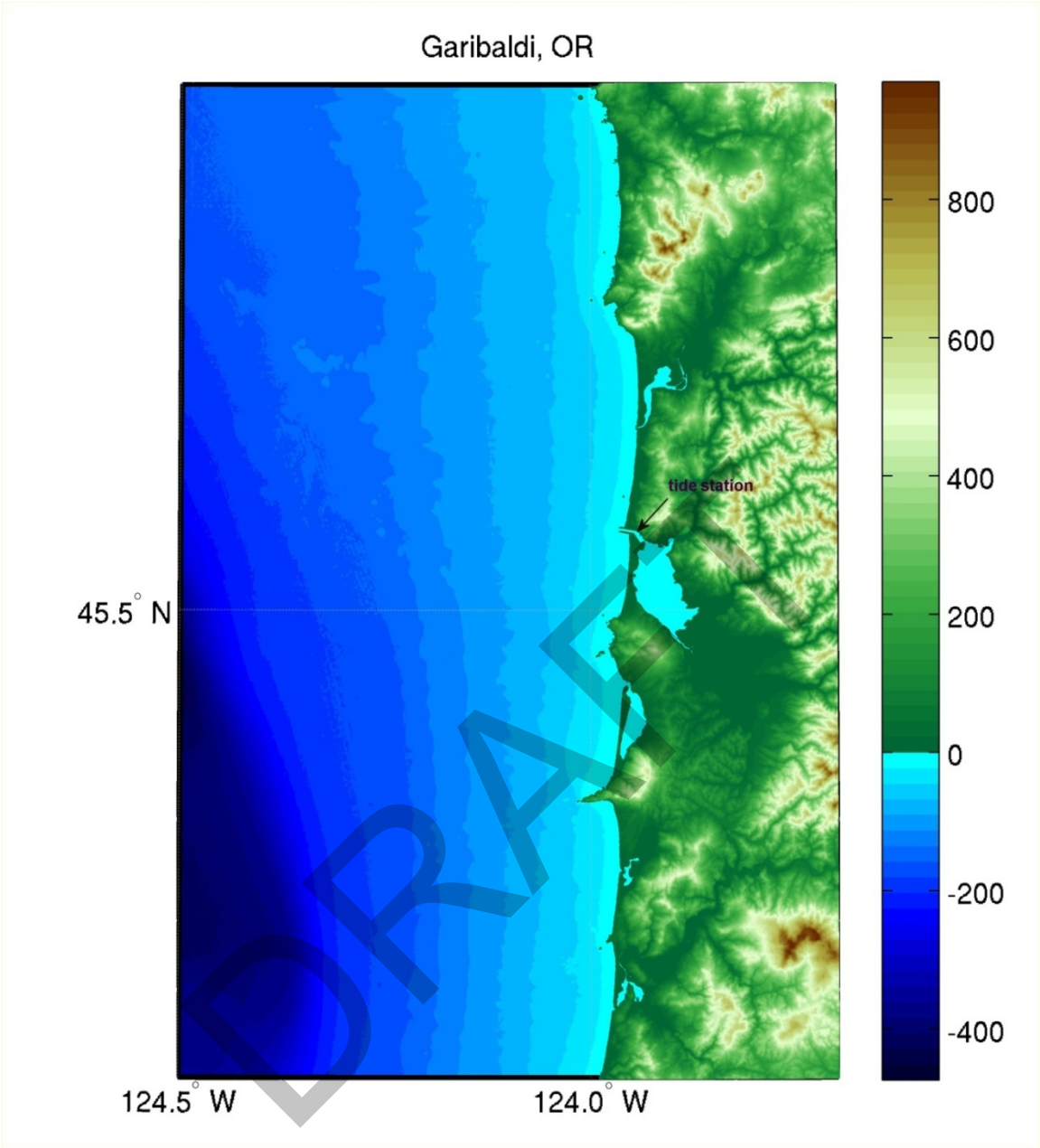

Figure 5 Contour plot of NGDC DEM for Garibaldi, OR

ncols	8641
nrows	9181
Xmin	-124.5000463000000
Ymin	45.0999537112000
Xmax	-123.7000463224000
Ymax	45.9499536874000
Zmin	-464.3545000000000
Zmax	969.8946999999999
cellsize	9.2592589999997e-05
nodata	-9999
new zonal cell size in meters	7.2132
new meridional cell size in meters	10.2958
east-west dimension in km	62.32214488
east-west dimension in meters	62322.14
north-south dimension in km	94.51568500
north-south dimension in meters	94515.69
number of nodes in grid	79333021

Table 1 Garibaldi, Oregon 1/3" arc second DEM attributes.

2.2 Reference Grids

For Grid A (both reference and forecast) use will be made of a previously prepared Grid A, supplied by Diego Arcas at PMEL. The computational cell size of this grid is 72 arc seconds. The cell size is approximately 2,160 meters. After passing it once through bathcorr.f (only one pass was necessary, using steepness = 0.5, and wave height = 0.5 m; these values of steepness and wave height values were also used for the other two reference grids when running bathcorr.f), we get Δt_A = 8.01 seconds. Figure 6 shows a contour plot of Grid_A_ref_72s_v1.dat, and the outlines of the finally adopted reference Grids B and C, discussed next.

For reference Grid B we took the entire NGDC DEM, and decimated it to 3 second resolution (read from the original 1/3 s). This gives a cell size of approximately 90 meters. Figure 7 shows a contour plot of the grid. After passing it once through bathcorr.f (only one pass was necessary), we get Δt_B = 0.969 seconds. From the NGDC DEM the reference Grid C was made. Figure 8 shows a contour plot of it, and This final version was called Grid_C_ref_2-3rds_v11.dat. Table 2 summarizes all the metadata for the three reference grids.

DRAFT

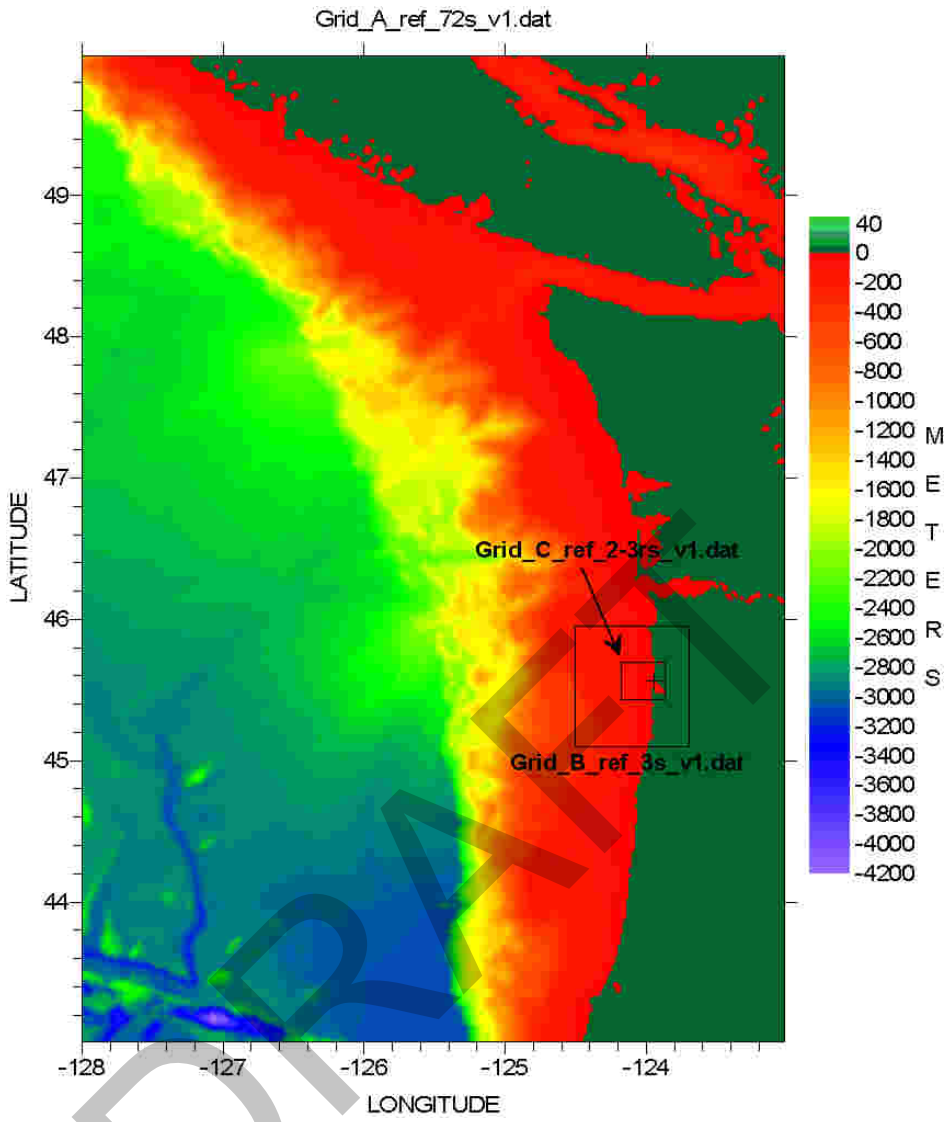

Figure 6 Contour plot of the reference Grid A. The outlines of the finally adopted reference Grids B and C are also shown. The black cross shows the location of the Warning Point.

DRAFT

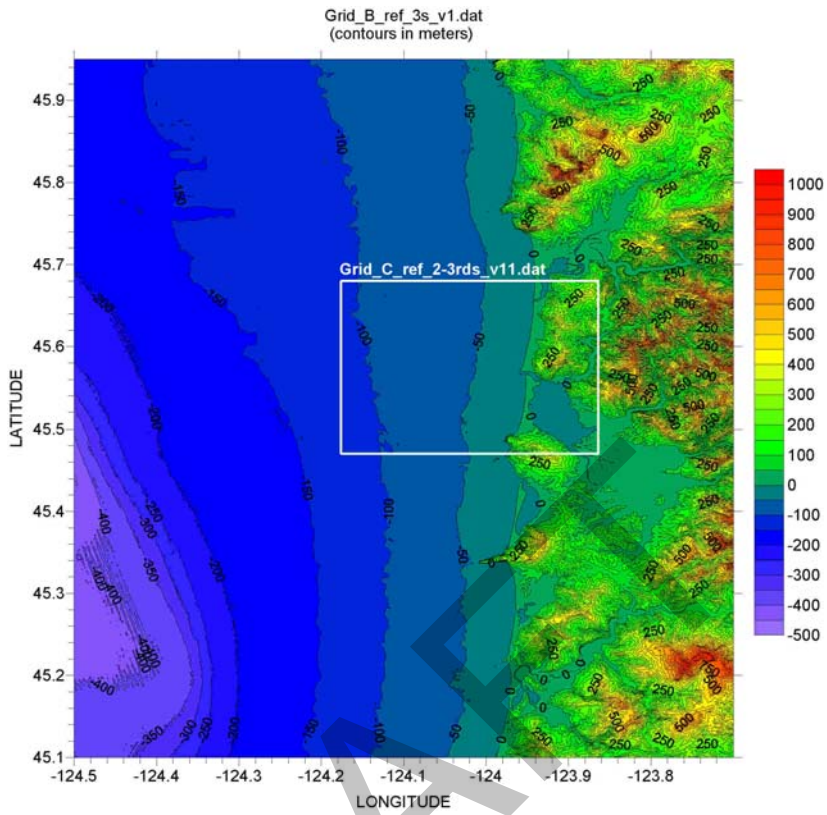

Figure 7 Contour plot of reference Grid B, and the outline of reference Grid C.

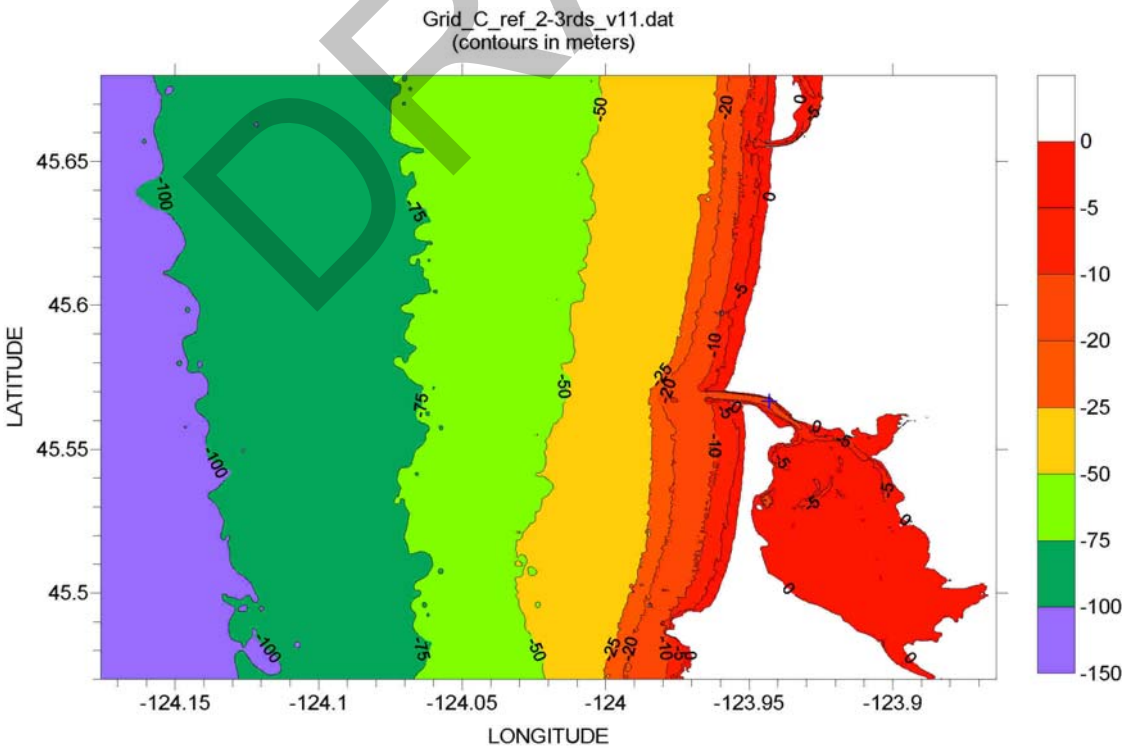

Figure 8 Contour plot of Grid_C_ref_2-3rds_v11.dat. Land values are not color filled. Blue cross shows location of Warning Point.

DRAFT

	A	B	C
Lat	49.99-123.02	45.0999537112-45.9499536874	45.46995370084-45.67995369496
Long	123.02-128	123.7000463224-124.5000463	123.8639352067-124.175972235
ncols	250	961	1686
nrows	350	1021	1135
Cellsize (arc sec)	72	3	2/3
X Grid spacing (degree)	0.02	0.00083333331	0.00018518518
Y Grid spacing (degree)	0.02	0.00083333331	0.00018518518
Zmin (m)	-4192.97	-460.32	-126.6279
Zmax (m)	0.5	967.2346	532.0929
Final file name	Grid_A_ref_72s_v1.dat	Grid_B_ref_3s_v1.dat	Grid_C_ref_2-3rds_v11.dat
Δt_A	8.01 seconds	0.969 seconds	0.41seconds

Table 2 Reference grid metadata for Garibaldi, Oregon

DRAFT

Several instabilities developed inside reference Grid C mainly because of the presence of offshore surface-piercing rocks in the open waters, because of the very steep slopes in the channel serving as the bay entrance (see Figures 9 and 10), and because of the several swampy areas surrounding the bay, areas containing narrow and steep channels.

It should be noticed that at the western end of the entrance channel its width is about 300 m, a width that remains approximately the same until the bend to the southeast. There it becomes wider, but at the channel end into the bay the width narrows down to about 210 meters (all of this estimated using Google Earth). Therefore, the western end of the entrance channel encompasses about 15 computational cells, while the eastern end encompasses about 8 cells (note the channel axis points in a SE to NW direction at the bay end).

2.3 Forecast model grids

After several attempts with different options the final forecast model grid was identical to the reference grid A. Table 3 summarizes the final parameters for the forecast model grids.

DRAFT

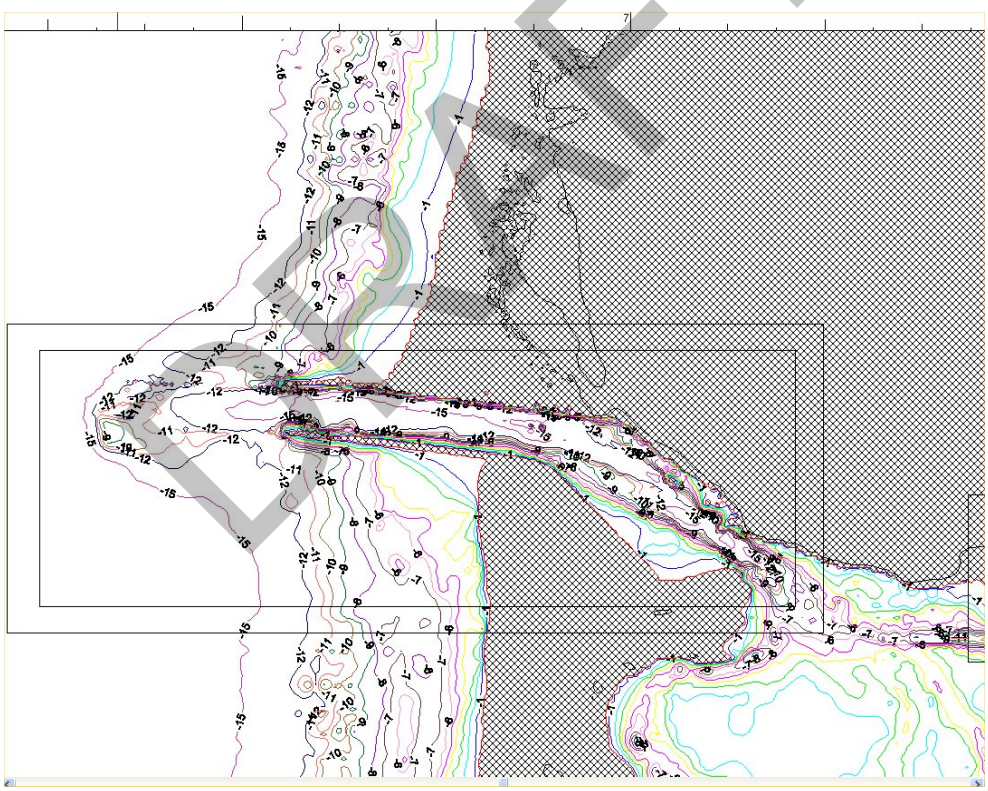

Figure 9 Zoom of the bay entrance, showing the steep slopes inside it.

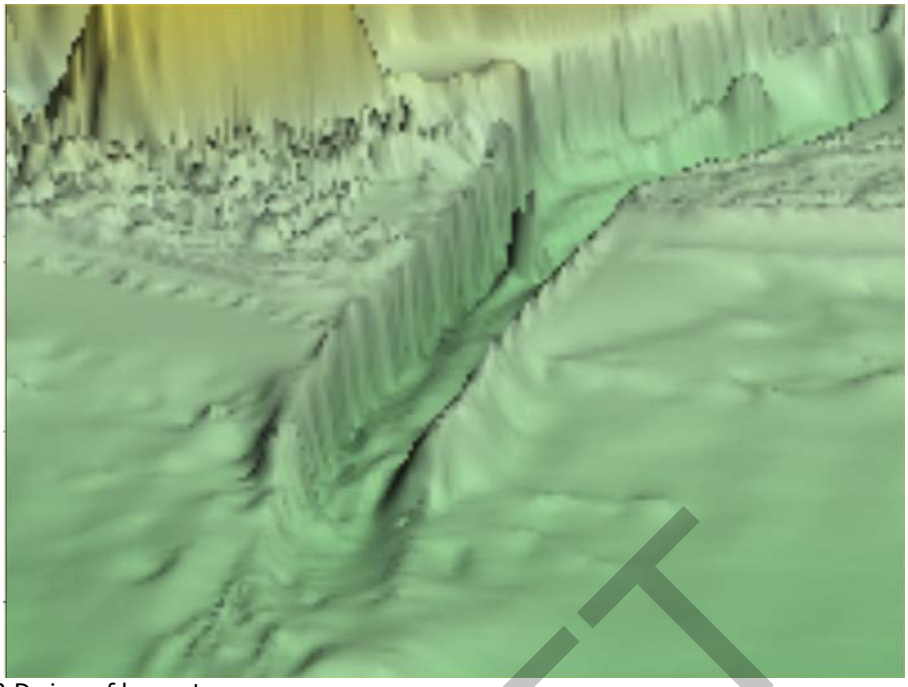

Figure 10 3-D view of bay entrance.

DRAFT

	A	B	C
Lat	49.99-123.02	45.351393494736-45.838697146013	45.48717592258-45.63495369622
Long	123.02-128	123.86004631792-124.35115741528	123.89115742816-124.0472685349
ncols	250	222	267
nrows	350	220	282
Cellsize (arc sec)	72	8	2
X Grid spacing (degree)	0.02	0.00222222216	0.00055555554
Y Grid spacing (degree)	0.02	0.0022251308277488	0.00055555554000001
Zmin (m)	-4192.97	-213.32	-69.99
Zmax (m)	0.5	897.691	530.8357
Final file name	Grid_A_opt_72s_v1.dat	Grid_B_opt_8s_v1.dat	Grid_C_opt_2s_v8.dat
Δt_A	8.01 seconds	3.8 seconds	1.65 seconds

Table 3 Forecast model grid parameters for Garibaldi.

DRAFT

Table4 shows the model setup for both RIM and forecast model for Garibaldi, OR.

Grid	**Region**	**Reference Inundation Model (RIM)**				**Stand-by Inundation Model (SIM)**		
		Coverage	Cell	Time		Coverage	Cell	Time
		Lat. [°N]	Size	Step		Lat. [°N]	Size	Step
		Lon. [°W]	["]	[sec]		Lon. [°W]	["]	[sec]
A	Strait of San Juan de Fuca	43.01 - 49.99 128.00-123.02	72	8.01		43.01 - 49.99 128.00-123.02	72	8.01
B	Central Oregon Coast	45.09995 - 45.94995 124.5000-123.700	3	0.969		45.3513 - 45.8386 124.3511 - 123.860	8	3.8
C	Garibaldi	45.4699 - 45.6799	2/3	0.41 (used .4)		45.4872 -45.6350		1.65 (used1.5)
		124.1760 - 123.8639				124.0472-123.8911		
Minimum offshore depth [m]			10			10		
Water depth for dry land [m]			0.15			0.1		
Manning coefficient			0.0009			0.0009		
CPU time for a 4-hour simulation (min)			717.7 to 839.95			8.97 to 9.08		

Table 4 MOST Model set up parameters for Garibaldi, OR

DRAFT

Figure 11 shows the RIM grid extents and Figure 12 shows the forecast model grid extents.

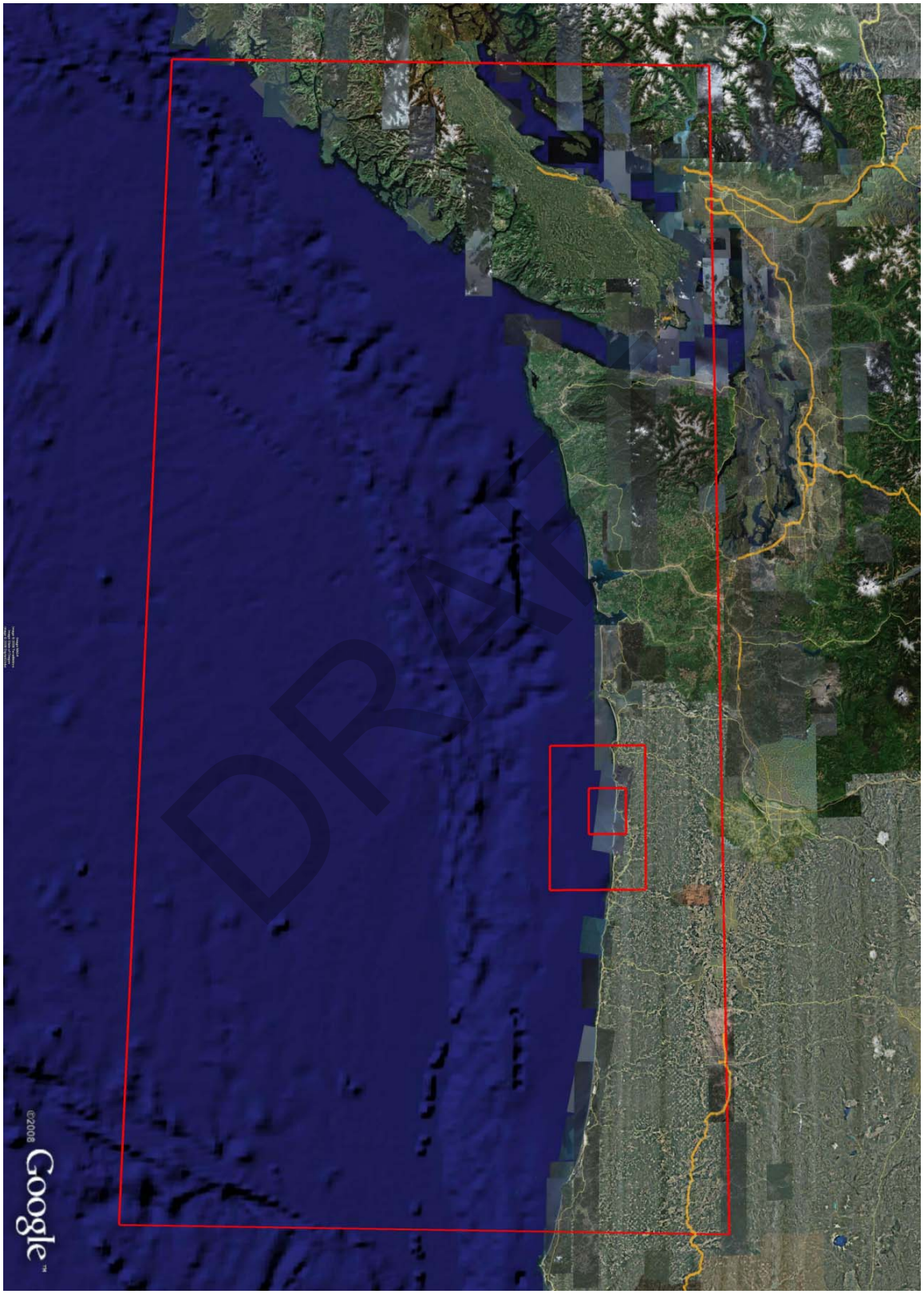

Figure 11 Outline of Reference grids (RIM)

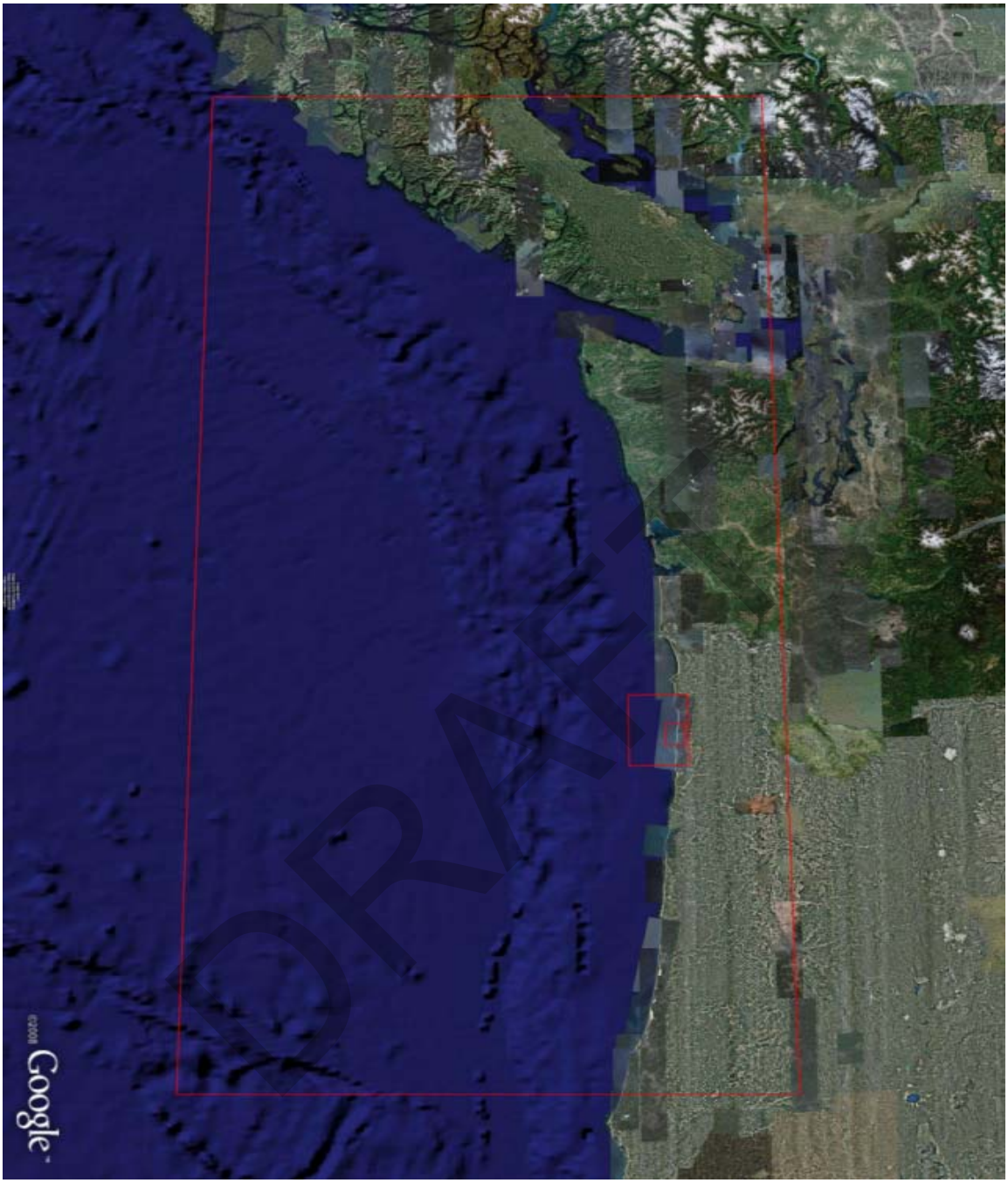

DRAFT

Figure 12 Outline of forecast grids (forecast model)

Event	Time (UTC)	Zone	M_w	Lon	Lat	Source
Chile		SASZ	7.6			0.81*a22+ 0.33*a23+ 0.11*b23
Peru	2007.08.15 23:40:57	SASZ	8.1	76.509W	13.354S	4.3×a9, 4.1×b9
Solomon	2007.04.01 20:40:40.7	NBSV	8.2	156.4E	7.96S	12.0×b10
Kuril	2007.01.13 04:23:48.2	KISZ	7.9	154.80E	46.18N	-3.82×b13
Kuril	2006.11.15 11:14:16	KISZ	8.1	154.32E	46.75N	4.0×a12+0.5×b12 +2.0×a13+1.5×b13
Tonga	2006.05.03 15:26:39	NZKT	8.1	174.164W	20.13N	8.44×b29
Rat Island	2003.11.17 06:43:07	AASZ	7.8	178.74E	51.13N	2.81×b11
Peru	2001.06.23 20:33:14	SASZ	8.2	73.31W	16.14S	5.7×a15+2.9×b16 +1.98×a16
Andreanof	1996.06.10 04:03:35.4	AASZ	7.8	176.847E	51.478N	2.4×a15+0.8×b16
Kuril	1994.10.04 13:22:58.3	KISZ	8.1	147.328E	43.706N	9.0×a20
Alaska	1964.03.28 03:36:14	AASZ	9.0	147.73W	61.04N	Tang et al.
Unimak	12:28 1946.04.01	AACC	8.5	163.5 W	52.75N	7.5*b23+19.7*b24+3.7* b25

Table 5 Historical events used to validate the Garibaldi forecast model

DRAFT

Name of Scenario	Scenario Number	Unit Source Combination
KISZ 1	1	A22-A31, B22-B31
KISZ 2	2	A1-A10, B1-B10
ACSZ 1	3	A12-A21, B12-B21
ACSZ 2	4	A22-A31, B22-B31
ACSZ 3	5	A38-A47, B41-B50
ACSZ 4	6	A56-A65, B56-B65
SASZ 1	7	A1-A10, B1-B10
SASZ2	8	A40-A49,B40-B49
NTSZ 1	9	A20-A29,B20-B29
NTSZ 2	10	A30-A39,B30-B39
NVSZ 4	11	A28-A37, B28-37
MOSZ 1	12	A1-A10, B1-B10
NGSZ 1	13	A3-A12, B3-B12
EPSZ 2	14	A6-A15, B6-B15
RNSZ 2	15	A12-A21, B12-B21
KISZ 3	16	A32-A41, B32-B41

Table 6 Artificial megatsunami sources uses for testing the Garibaldi, OR forecast model.

DRAFT

3.0 Results

3.1 Model Validation

Two time histories (Tonga 2006 and Kuril 2006) of recorded tsunamis at the Garibaldi tide gauge were used for model validation. Both records were obtained through Ms. Nazila Merati of PMEL/NOAA.

3.1.1 Tonga May 2006

Figure 13 shows the original time history for the Tonga, May 2006, event. The origin of the time axis is the moment of the earthquake. Figure 14 zooms in into the approximate moment when the maximum tsunami waves reached the tide gauge. To extract the tsunami signal the data was passed through a Matlab program supplied by Dr. Diego Arcas (PMEL) which does the following:

1. Demeans the signal

2. Fits a spline using the function (in the Spline Toolbox) *csaps(ts,csig,p)*, where *ts* is the vector of time values, *csig* is the vector containing the sea surface elevation signal, and *p* is the smoothing parameter. The *p* values varies between 0 and 1, with $p = 0$ corresponding to a least-squares straight line fit to the data, while, at the other extreme, i.e., for $p = 1$, is the variational, or `natural' cubic spline interpolant. For this time history a values of p=0.000000001 was used.

3. The spline fit is then subtracted from the demeaned original signal to get the tsunami signal.

DRAFT

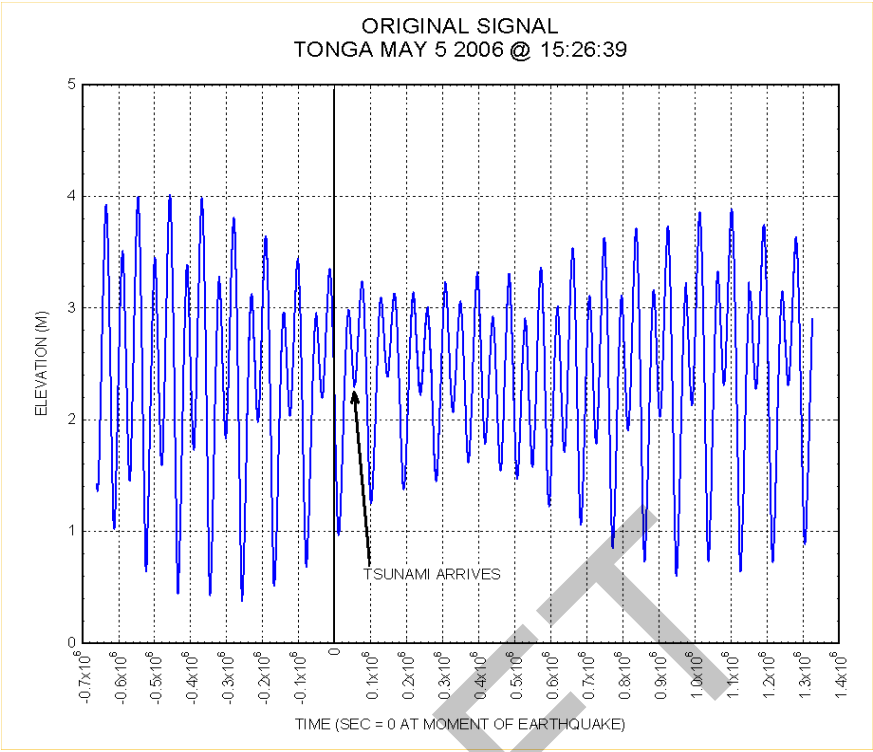

Figure 13 Original time history for 2006 Tonga event.

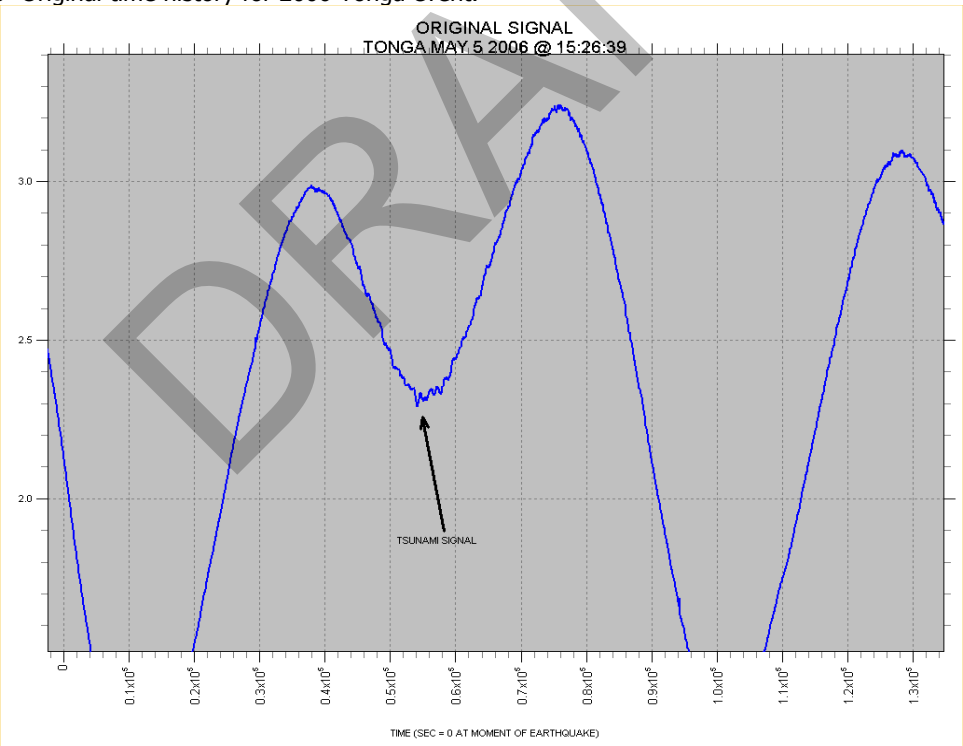

Figure 14 Zoom of above figure.

DRAFT

Figure 15 shows the result of this processing. It can be seen that it is somewhat subjective deciding when the first tsunami wave arrives. This is in large part due to the presence of a quasi-periodic signal with a period on the order of 1 hour, which cannot be due to the tsunami since it is present right from the moment when the earthquake occurred. But a few minutes after hour 12 (more exactly, 12.2119 hours) we can notice the presence of higher frequency, and amplitude, waves which could signal the arrival of the first tsunami wave. The amplitude (half the wave height) of the "tsunami waves" is on the order of 0.01 – 0.015 meters.

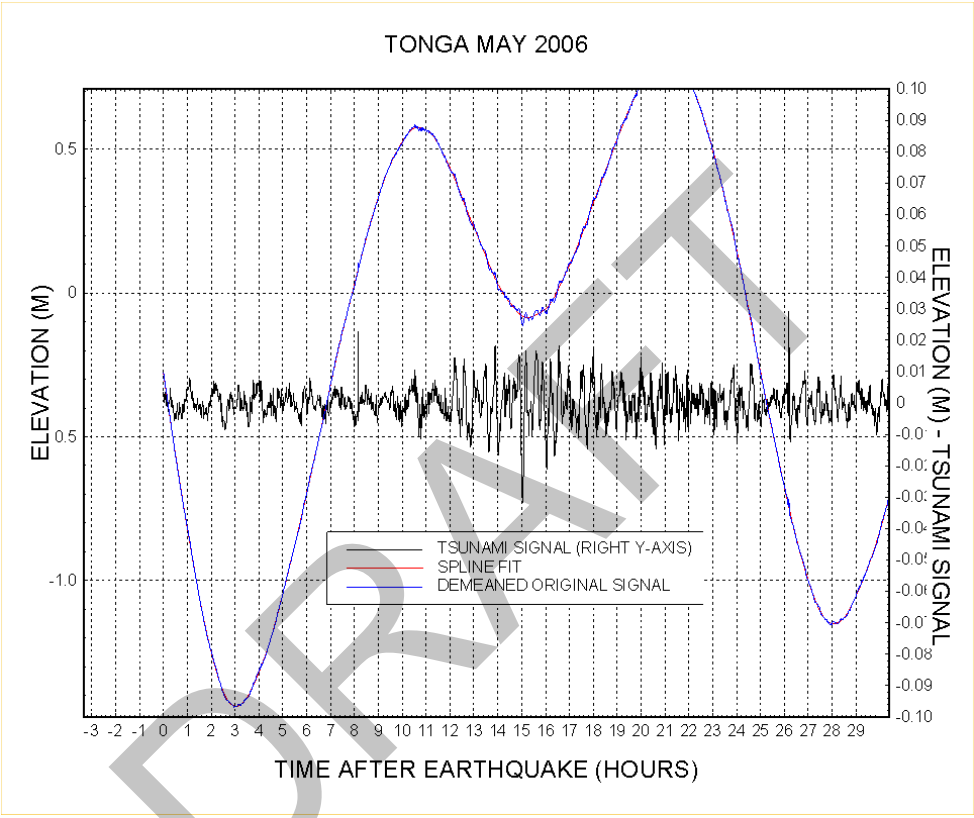

Figure 15 Demeaned original series, spline fit, and tsunami signal.

Figure 16 shows the observed tsunami signal (Tonga 2006) compared with the MOST results for both RIM and forecast model grids. If we compare the time of arrival of the peak of the first tsunami wave from MOST and the time corresponding to the highest of the three small peaks on the crest of the first arriving observed wave we get that the first wave of the observed tsunami arrives about 8 minutes after the model's first wave.

The first 5 MOST waves have a period varying between 12 and 23 minutes (measured from peak to peak), while the first 5 observed waves have a period (measured using the downward zero-crossing method due to their irregular shape) varying between 19 and 35 minutes. These waves certainly are of smaller period than that of the oscillations seen from time zero in that same series (observed tsunami) which precede the tsunami arrival. The amplitudes of both the RIM and forecast model waves are 2 to 3 times larger than the amplitude of the observed waves.

DRAFT

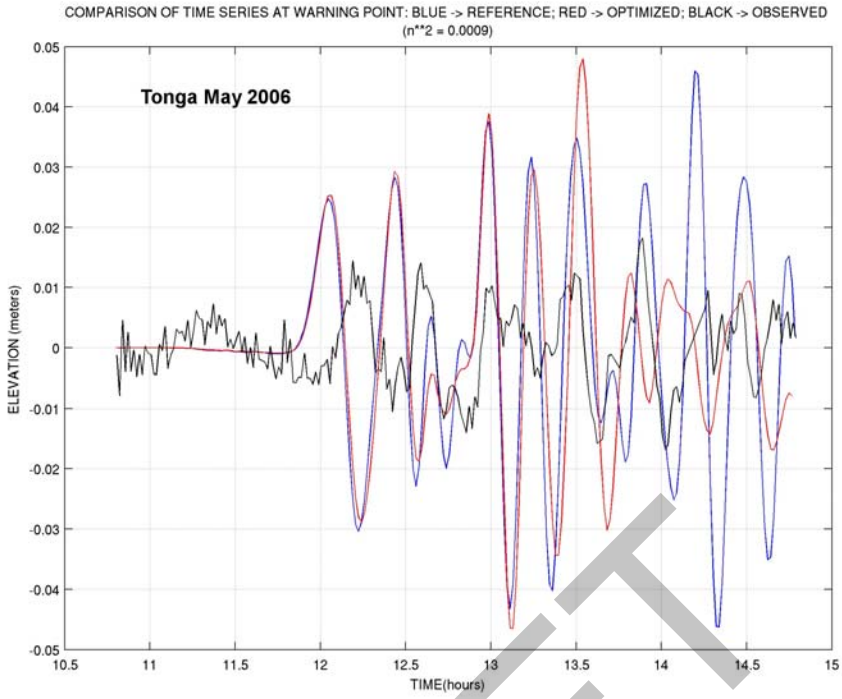

Figure 16 Time history comparison. Blue curve is the RIM, red curve is the forecast model, and black curve is the observed event.

DRAFT

3.1.2 Kuril Nov 2006

Figure 17 shows a plot of the original time series for the Kuril 2006 event as recorded at the Garibaldi tide gauge. We can notice the presence of (6) outliers at ebb tide during the presence of the tsunami signal. Figures 18 and 19 show zoom in around this time interval. This implies that before fitting a spline (as done to the Tonga event) in order to extract the tsunami signal, we must somehow "correct" these outliers. This was done arbitrarily adding the value of 0.53923 to the six elevation values described as outliers. Figure 19 shows a zoomed image of the problem area, with the black curve and crosses showing the original data and the blue curve and X's showing the edited data.

Figure 20 shows the results of the processing done to extract the tsunami signal. It can be seen that in this case the spline fit is not as smooth as for the Tonga 2006 event. And the tsunami signal is much more irregular also, which makes it difficult to pinpoint when did the real tsunami arrived.

Figure 20 gives the impression that the highest tsunami waves reached the tide gauge about 12 hours after the earthquake, while Figure 21 shows that the first wave from MOST arrived 8.43262 hours after the earthquake. With such a low signal-to-noise ratio, and a de-tiding spline fit that is certainly not as smooth as for the Tonga 2006 event, it is difficult to pinpoint when the real tsunami arrived. And, again, the model's amplitudes are larger than for the real event.

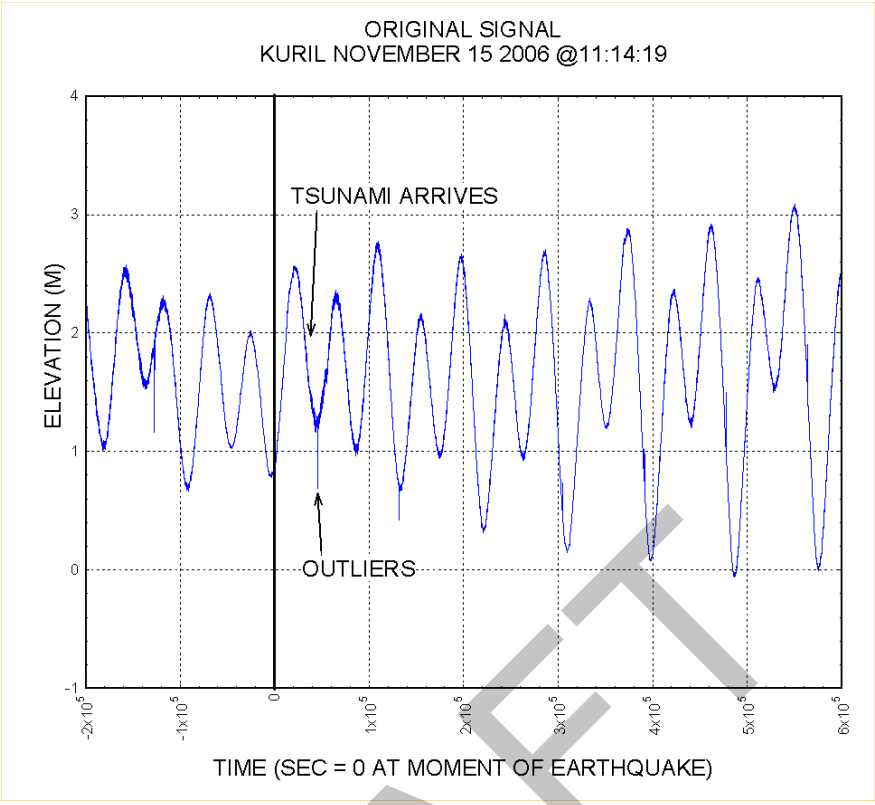

Figure 17 Original time history for 2006 Kuril event.

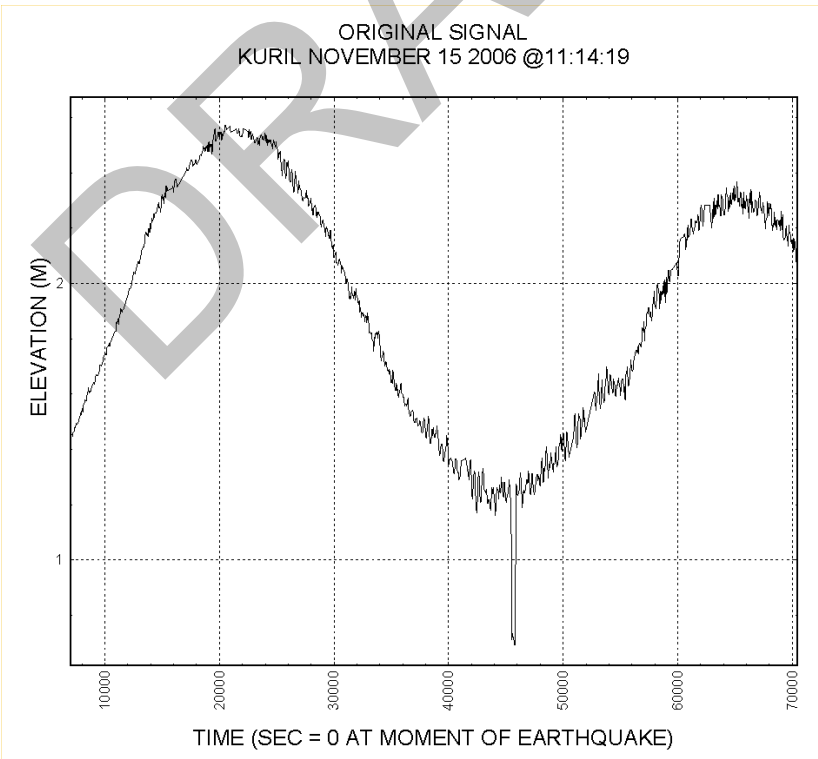

Figure 18 Zoom of tsunami event.

DRAFT

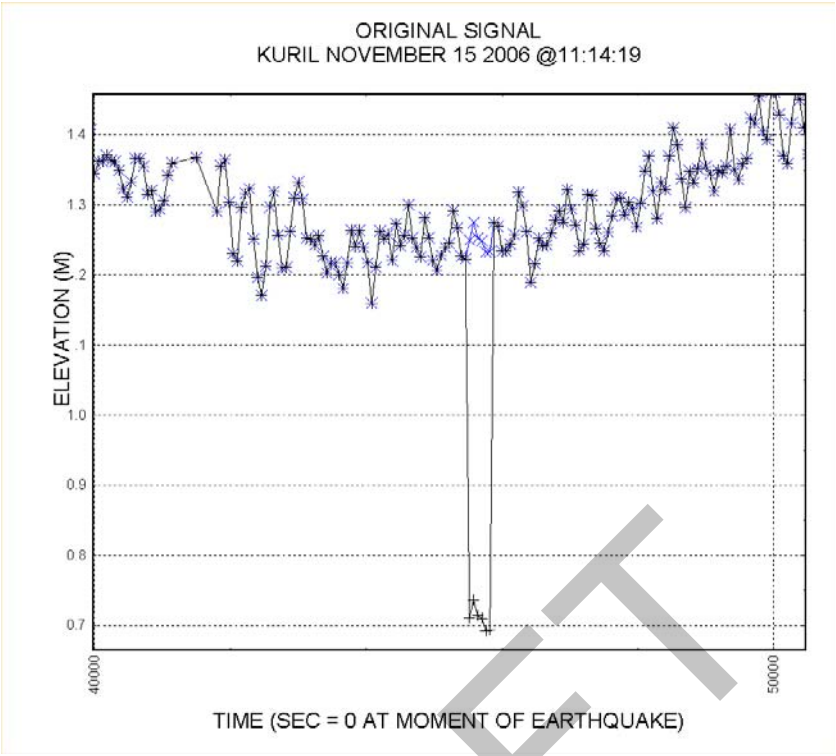

Figure 19 Zoom of above figure, showing the outliers (blue) and the "corrected" signal (black).

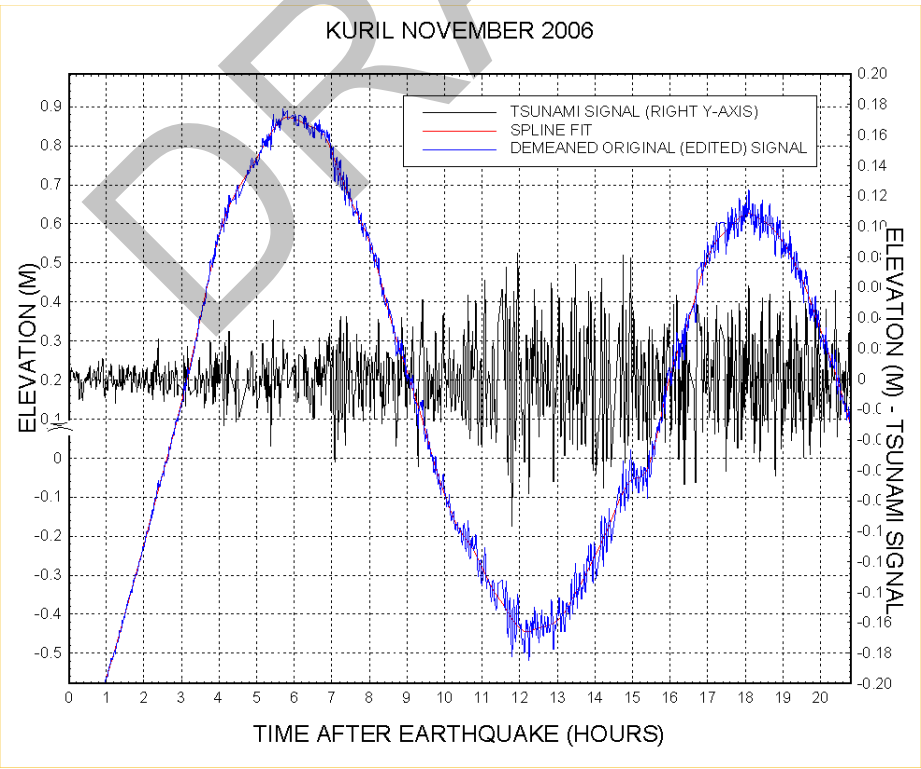

Figure 20 Demeaned original series, spline fit, and tsunami signal.

DRAFT

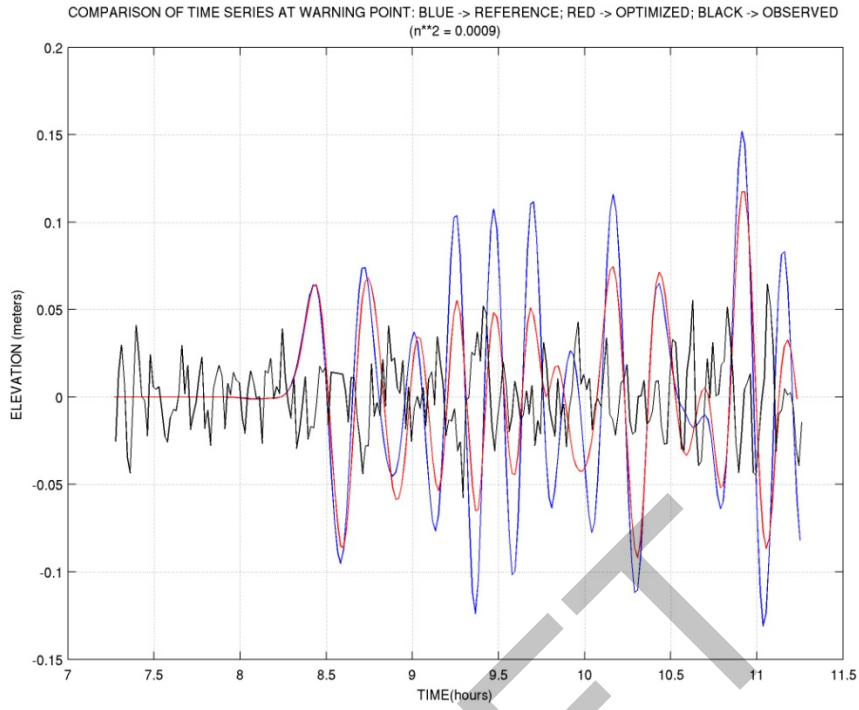

Figure 21 Time history comparison. Blue curve is the RIM, red curve is the forecast model, and black curve is the observed event**.**

3.2 Model Stability and Reliability

As Figures 9 and 10 show, the entrance channel has very steep slopes that generated instability problems. Bathcorr.f was used with steepness parameter (SP) down to 0.1 (the smaller the value, the more the smoothing), but the problem remained. Therefore, several local smoothing attempts were made using the Surfer software package, based on a Gaussian shape smoothing matrix. For example, the inner rectangle in Figure 2-9 shows where 5 smoothing passes were made with a Gaussian filter of 3 columns by 3 rows. The filter weights are

1	2	1
2	4	2
1	2	1

In between the inner and outer rectangle the same filter is used, but with a smaller amount of passes, in this specific case, 2. This serves as a buffer area to more smoothly make the transition from the area of high smoothing to the area of no smoothing at all.

Since additional smoothing was required, it was done locally using a Surfer script as explained in section 2.1 above. Another troublesome area was located very close to the southern boundary of the reference Grid C, where large offshore rocks are located. Again, these were taken care of by Surfer smoothing. Another instability area was seen in the marina area of the city (Garibaldi), again taken care of by local smoothing.

DRAFT

Finally, the instability moved to what looks as tidal marshes on the southeast region of the bay (see Figure 2). It should be mentioned that, especially for the later instabilities, the model would not crash, but it would finish and produce an output. But the time history at the WP looked strange. One way of noticing the location of the instability was by plotting the maximum wave heights irrespective of time, and noticing that the maximum runup was occurring at the SE region of the bay, in the swampy area. Since I see no reason why the maximum runup should occur along the SE corner of the bay, instead of the open shores of the grid, I assumed that as long as the maximum runup was occurring at that corner that this was the source of an instability that propagated all over the computational grid and contaminated the signal at the WP (without crashing the execution of MOST). And by locally smoothing the SE corner of the bay the maximum runup moved to outside the bay, and we could immediately see that the signal at the WP did become more tsunami-like. As a matter of fact, since the forecast Grid C did not include that SE corner (due to CPU time limitations), it produced a signal at the WP that looked tsunamigenic, and completely different than the signal output by the reference Grid C that included the SE corner (and which included the maximum runup location). Once the SE corner was smoothed, the signal at the WP in the reference Grid C became a much better match of the forecast signal at the WP.

3.3 Results of Tested Events

Figures 22 to 32 show plots of the time series comparison between the RIM and forecast model for each of the events listed in Table 5. The name of the event is listed in the figure captions. The Root Mean Square Error is also listed along the top of each figure.

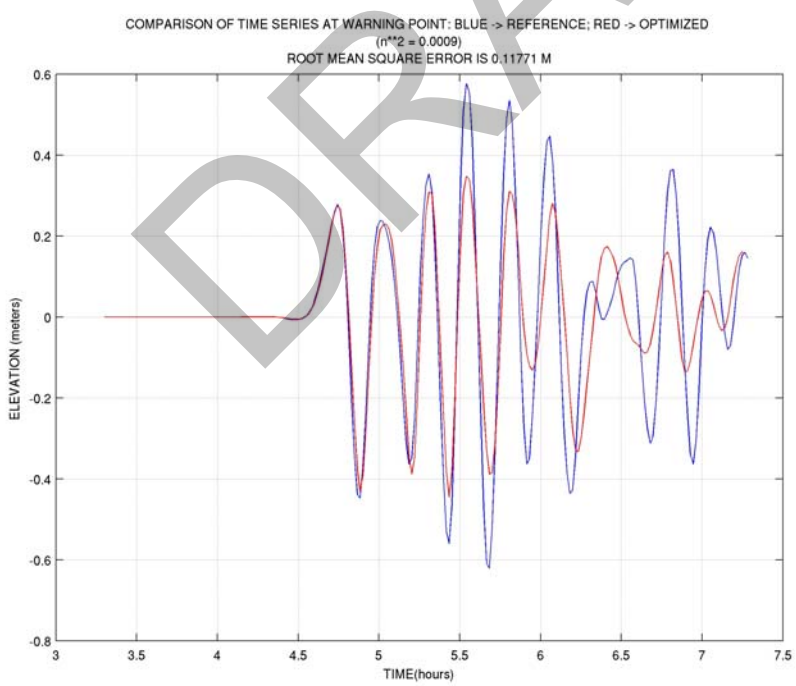

Figure 22 Time series comparison RIM vs. forecast model for 1946 Unimak event.

DRAFT

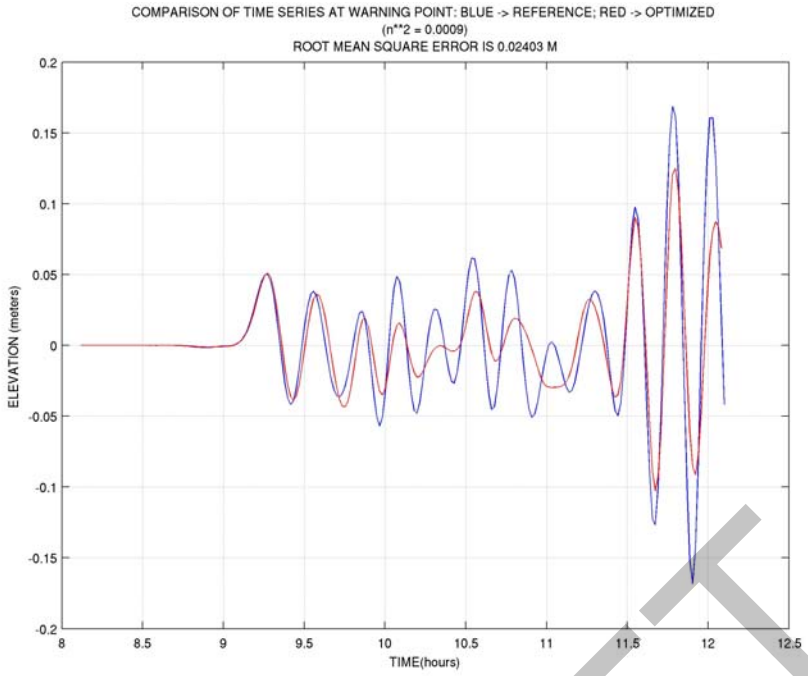

Figure 23 Time series comparison RIM vs. forecast model for 1994 Kuril event.

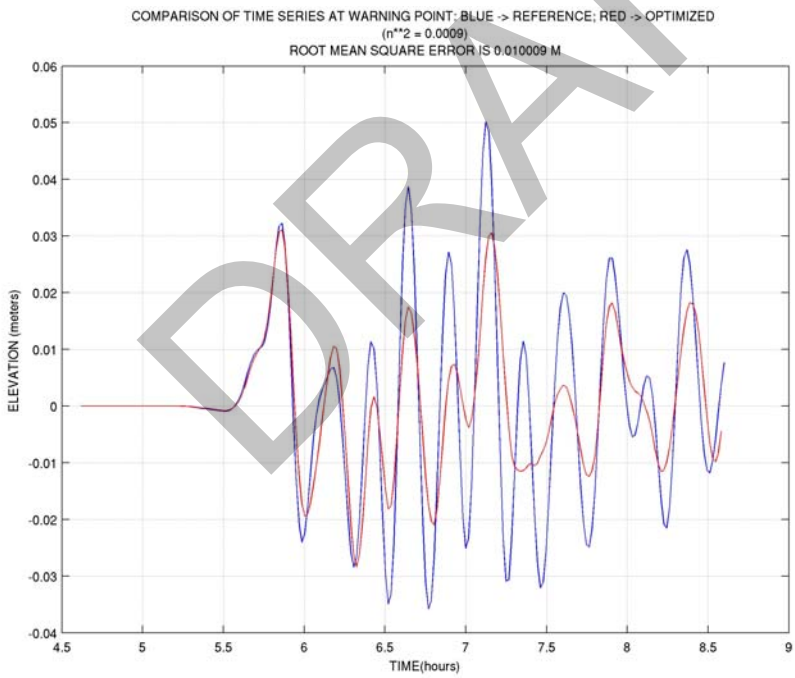

Figure 24 Time series comparison RIM vs. forecast model for 1996 Andreanof event.

DRAFT

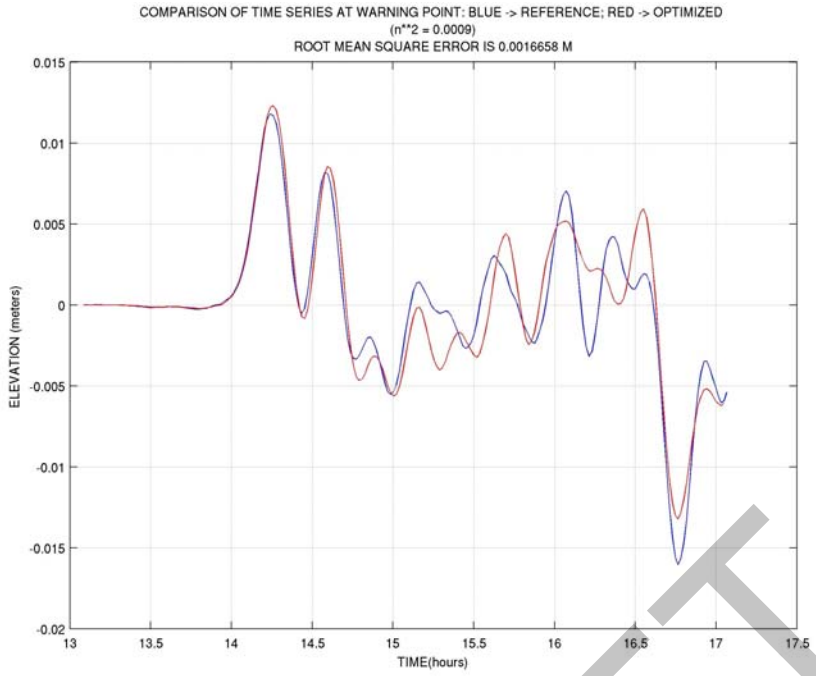

Figure 25 Time series comparison RIM vs. forecast model for the 2001 Peru event.

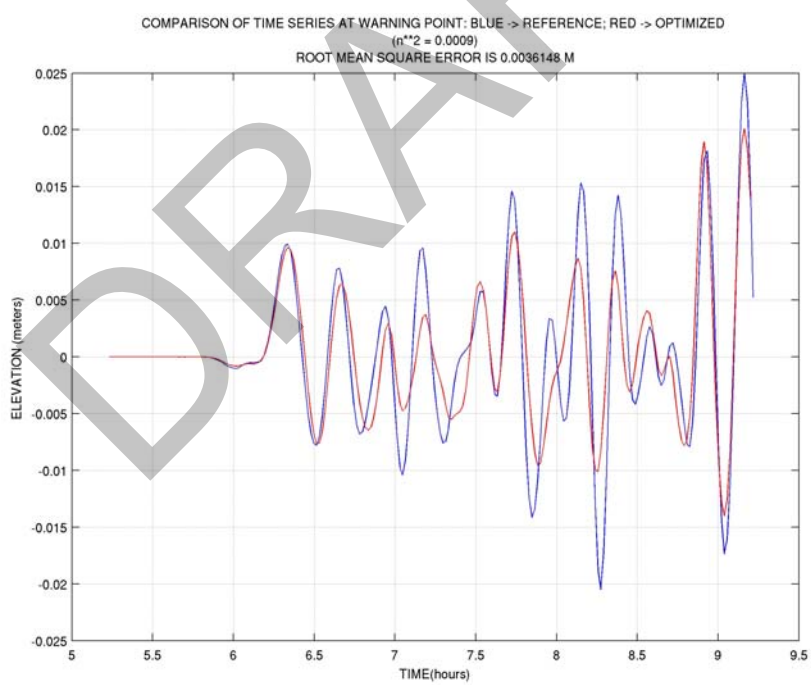

Figure 26 Time series comparison RIM vs. forecast model for the 2003 Rat Island event.

DRAFT

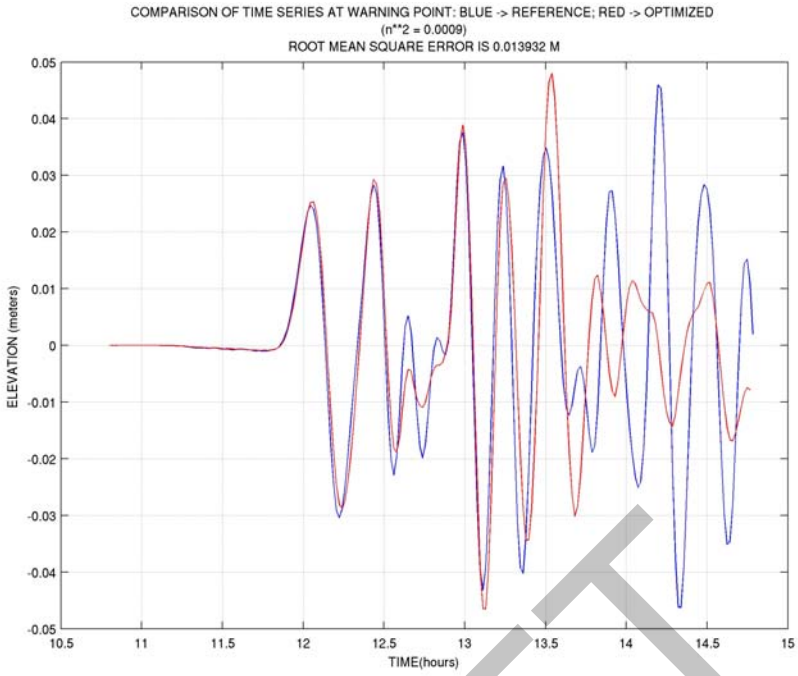

Figure 27 Time series comparison RIM vs. forecast model for 2006 Tonga event.

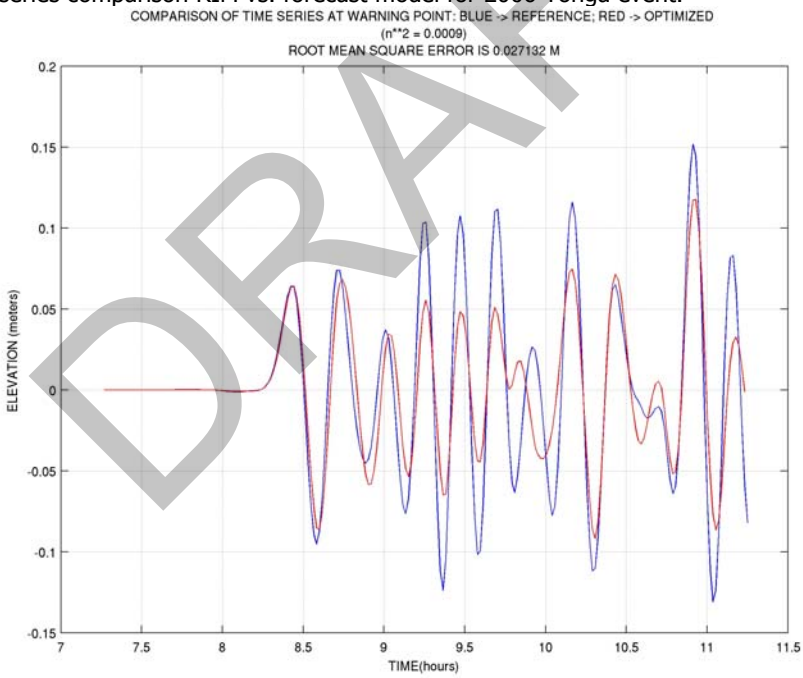

Figure 28 Time series comparison RIM vs. forecast model for the 2006 Kuril event.

DRAFT

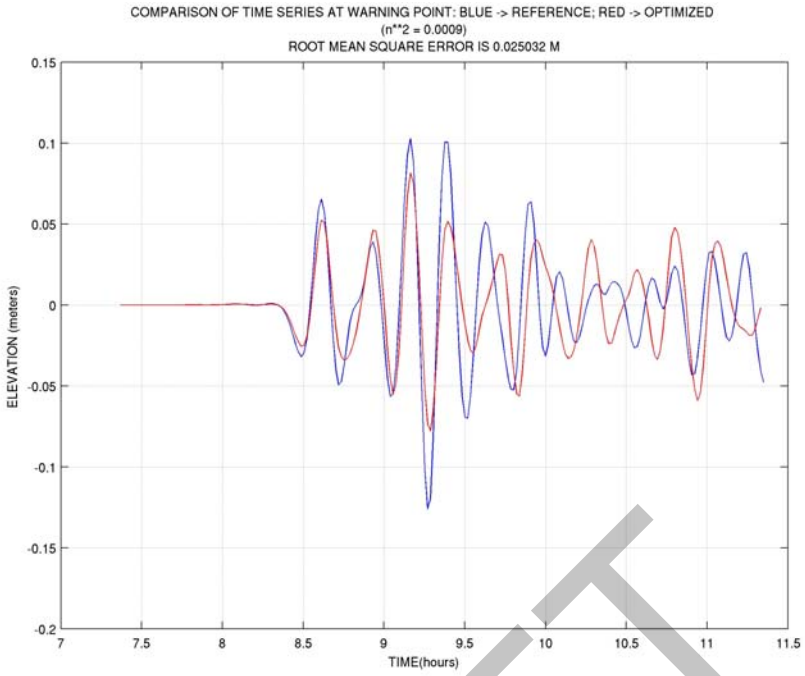

Figure 29 Time series comparison RIM vs. forecast model for the 2007 Kuril event.

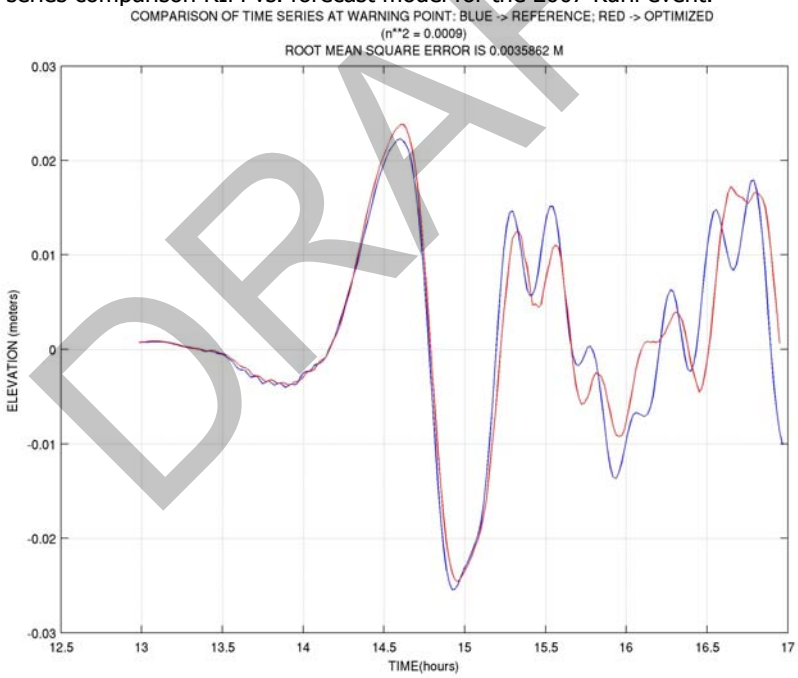

Figure 30 Time series comparison RIM vs. forecast model for 2007 Solomon event.

DRAFT

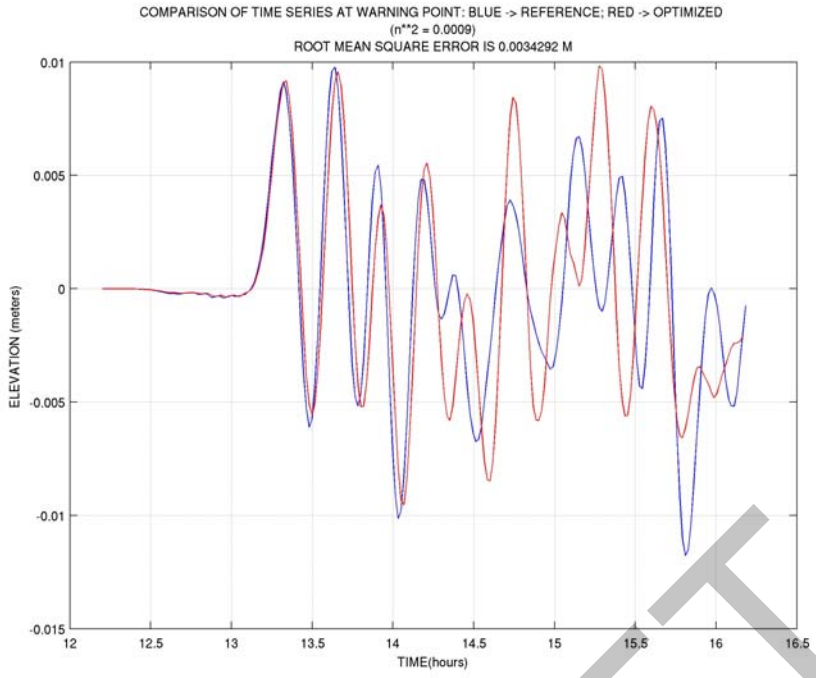

Figure 31 Time series comparison RIM vs. forecast model for 2007 Peru event.

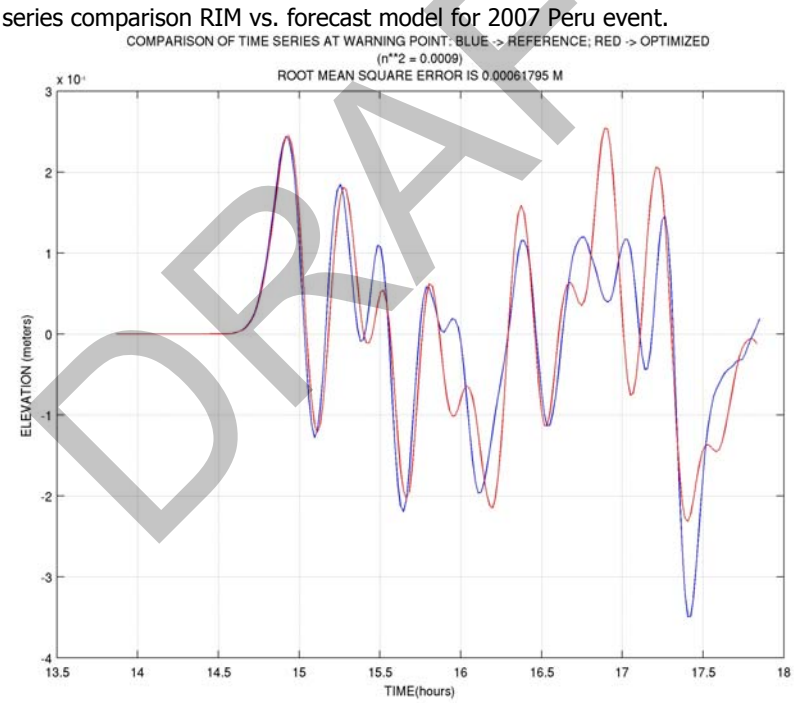

Figure 32 Time series comparison RIM vs. forecast model for the 2007 Chile event.

DRAFT

Figure 33 to 43 show the maximum sea surface elevations irrespective of time (what the storm surge community calls the Maximum Envelope of Highest Water or MEOHW) for each one of the artificial tsunamis given in Table 6. A cross is placed at the WP location, while a pentagram shows the location where the maximum runup occurred. The event name is shown along the top of each figure.

DRAFT

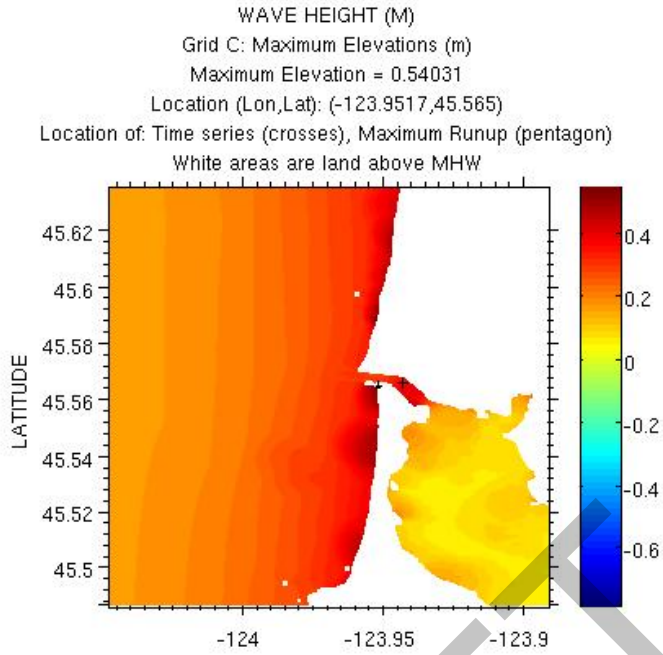

Figure 33 Maximum Envelope of Highest Water for the 1946 Unimak event.

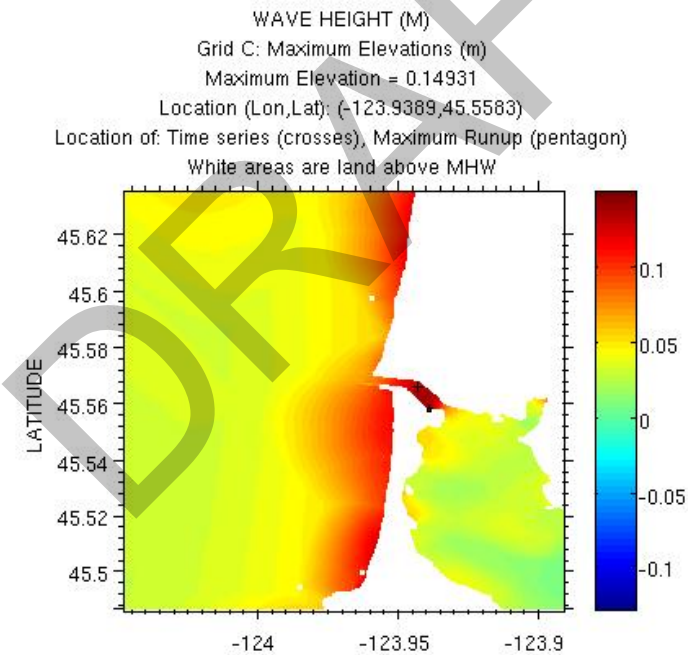

Figure 34 Maximum Envelope of Highest Water for the 1994 Kuril event.

DRAFT

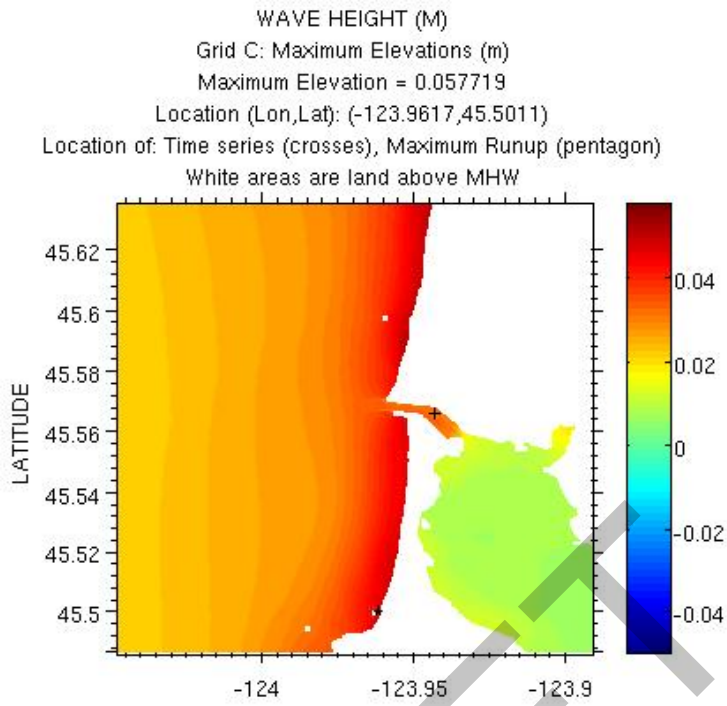

Figure 35 Maximum Envelope of Highest Water for the1996 Andreanof event.

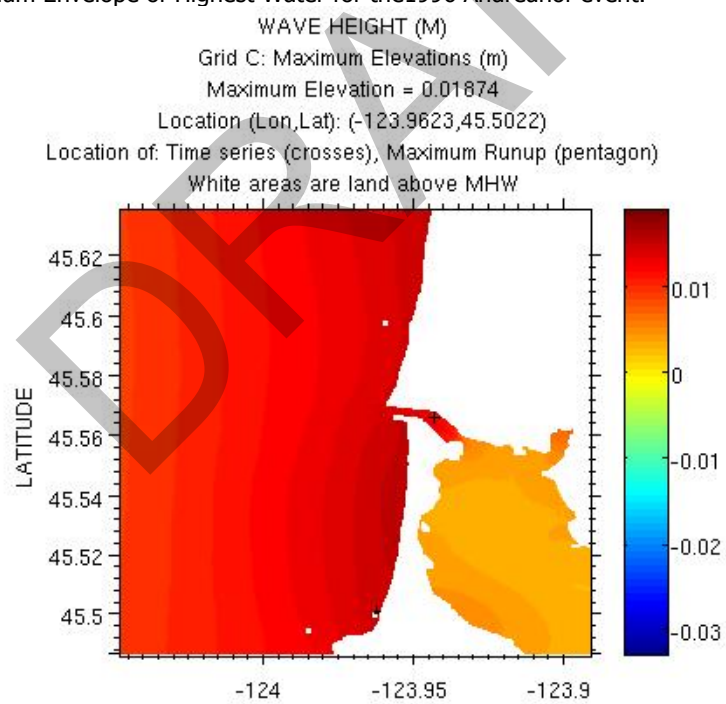

Figure 36 Maximum Envelope of Highest Water for the 2001 Peru event.

DRAFT

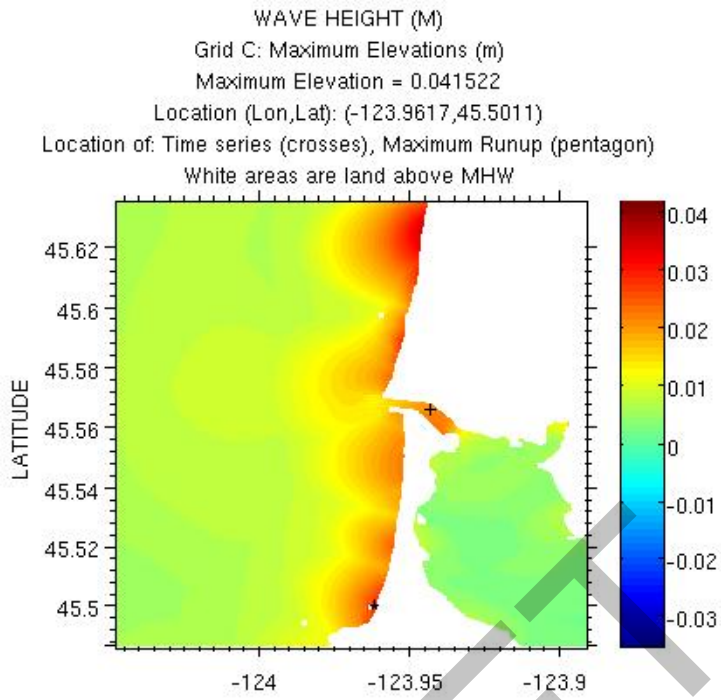

Figure 37 Maximum Envelope of Highest Water for the 2003 Rat Island event.

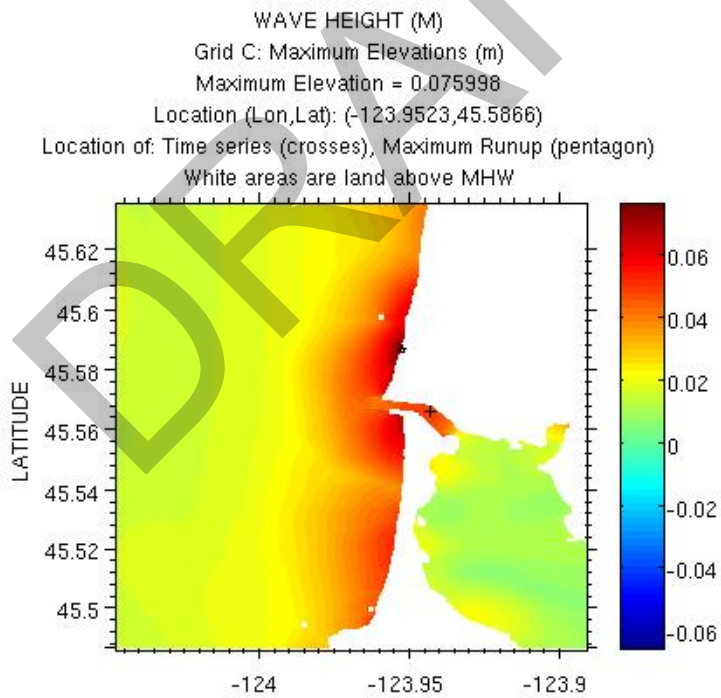

Figure 38 Maximum Envelope of Highest Water for the 2006 Tonga event.

DRAFT

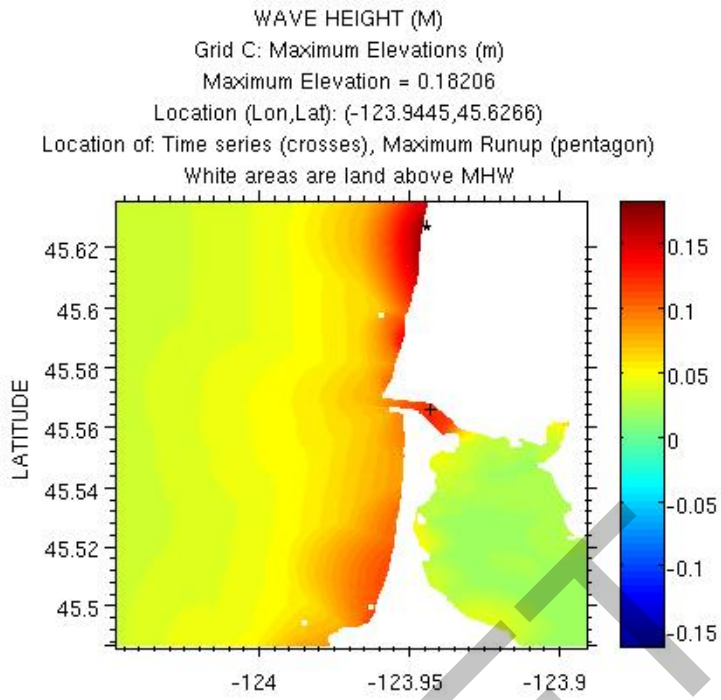

Figure 39 Maximum Envelope of Highest Water for the 2006 Kuril event.

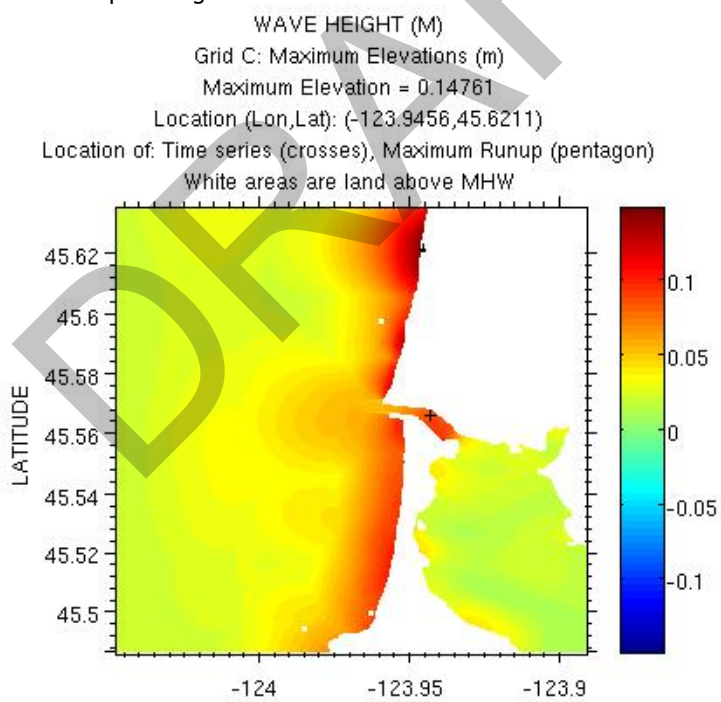

Figure 40 Maximum Envelope of Highest Water for the 2007 Kuril event.

DRAFT

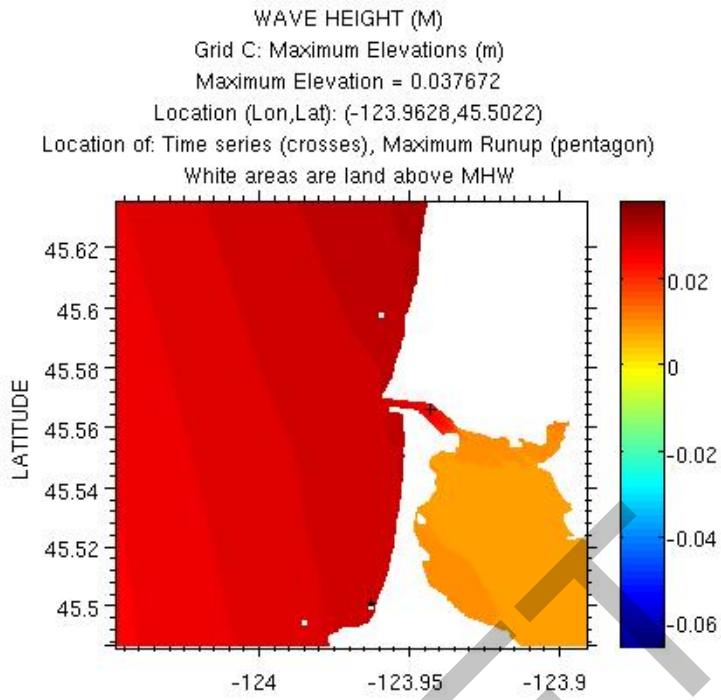

Figure 41 Maximum Envelope of Highest Water for 2007 Solomon event.

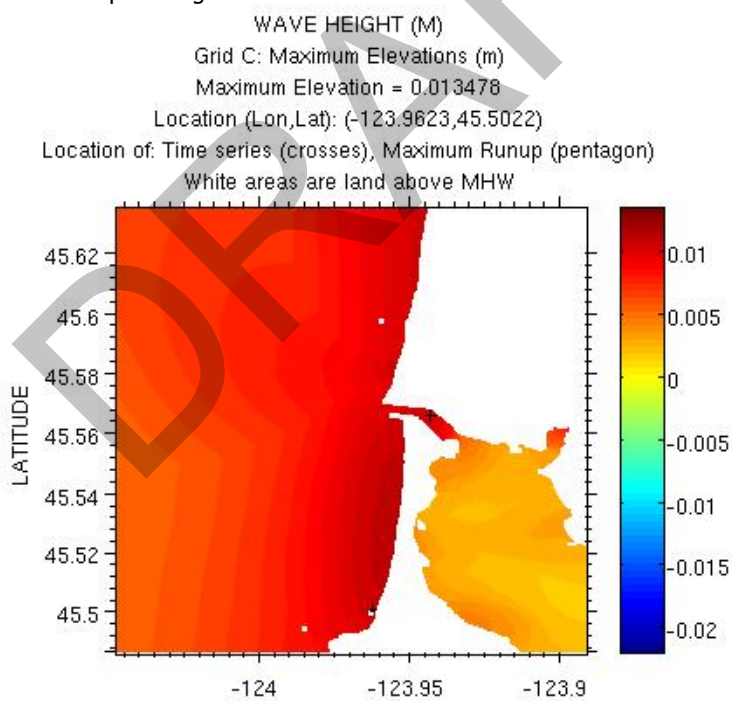

Figure 42 Maximum Envelope of Highest Water for the 2007 Peru.

DRAFT

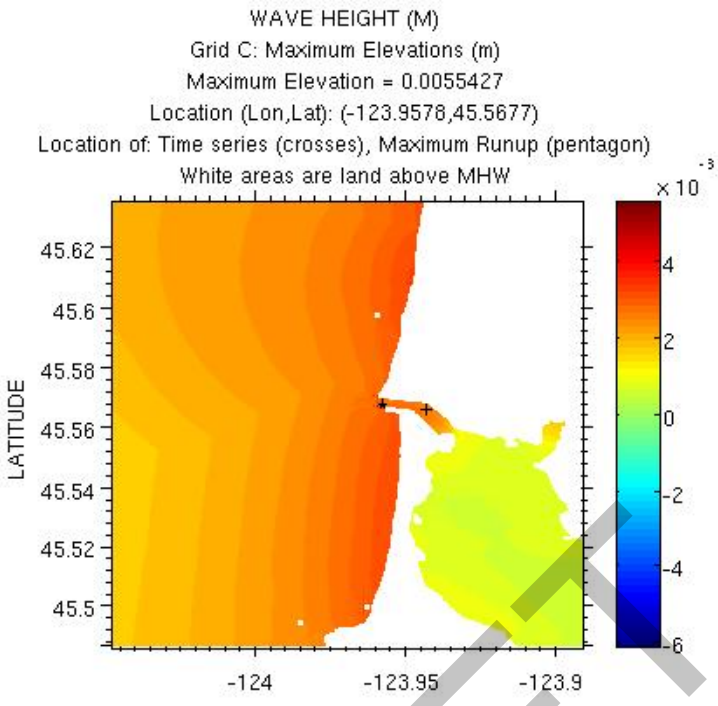

Figure 43 Maximum Envelope of Highest Water for 2007 Chile event.

4.0 Discussion

In our search for a stable version of the reference Grid C, eleven grids were tested, finally settling for the grid called Grid_C_ref_2-ds_v11.dat. The string "2-3rds" means that the computational cell size is 2/3 of an arc second (approximately 20 meters; see Table 8).

As can be seen from some of the Figures 22 to 32, which show the comparison between the reference and forecast tsunami signal at the WP, for some of the events both the reference and forecast signals increase their amplitude with time while maintaining a good match, but at some moment (after the third or fourth wave) the reference signal becomes larger than the forecast signal. In order to see if we could come up with an forecast grid that prevented this mismatch in amplitude to occur, several attempts were made using different forecast grids, and combinations amongst them. For the attempts listed below we used as source the event having the highest wave amplitudes, T01_1946Unimak_j1_weco. RMSE stands for Root Mean Square Error assuming that the reference results are the standard. These are shown in the follow figures and annotations.

DRAFT

Attempt_1: **Grid_A_opt_72s_v1.dat (nrows=383,ncols=289,nodes=110,687,** Δt_A = 8.01 s)

Grid_B_opt_8s_v1.dat (nrows=220,ncols=222,nodes=488740, Δt_B = 3.80 s)

Grid_C_opt_2s_v1.dat (nrows=181,ncols=689,nodes=124709, Δt_C = 1.08 s)

Δt used = 0.93, CPU time = 19.8 minutes, RMSE = 0.125 m

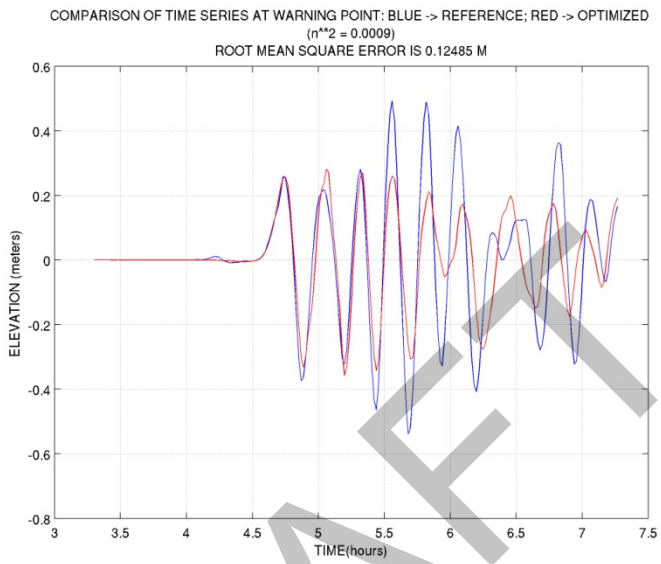

Figure 44 Attempt 1 for T01_1946Unimak_j1_weco.

Notice that the first 3 peaks match well, but the 4th, 5th, and 6th in the forecast attempt become smaller than for the reference run. This is something that we will attempt to improve in the attempts that follow, while at the same time trying to keep the CPU time below 10 minutes.

For Attempt_2 we increased the north-south coverage of Grid C and at the same time decreased its east-west extension.

Attempt_2: **Grid_A_opt_72s_v1.dat (nrows=383,ncols=289,nodes=110,687,** Δt_A = 8.01 s)

Grid_B_opt_8s_v1.dat (nrows=220,ncols=222,nodes=488740, Δt_B = 3.80 s)

Grid_C_opt_2s_v2.dat (nrows=350,ncols=354,nodes=123900, Δt_C = 1.458 s)

Δt used = 1.4, CPU time = 14.22 minutes, RMSE = 0.132 m

DRAFT

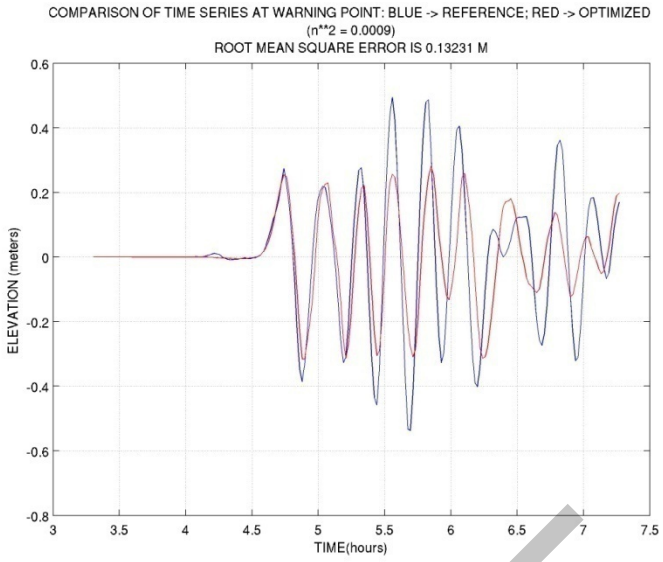

Figure 45 Attempt 2 for T01_1946Unimak_j1_weco.

For Attempt_3 we used the same grids as Attempt_1, but in the *.in file the number of steps in Grid B was increased from 2 to 3.

Attempt_3: **Grid_A_opt_72s_v1.dat (nrows=383,ncols=289,nodes=110,687,** Δt_A = 8.01 s)

Grid_B_opt_8s_v1.dat (nrows=220,ncols=222,nodes=488740, Δt_B = 3.80 s)

Grid_C_opt_2s_v1.dat (nrows=181,ncols=689,nodes=124709, Δt_C = 1.08 s)

Δt used = 0.93, CPU time = 18.67 minutes, RMSE = 0.125 m

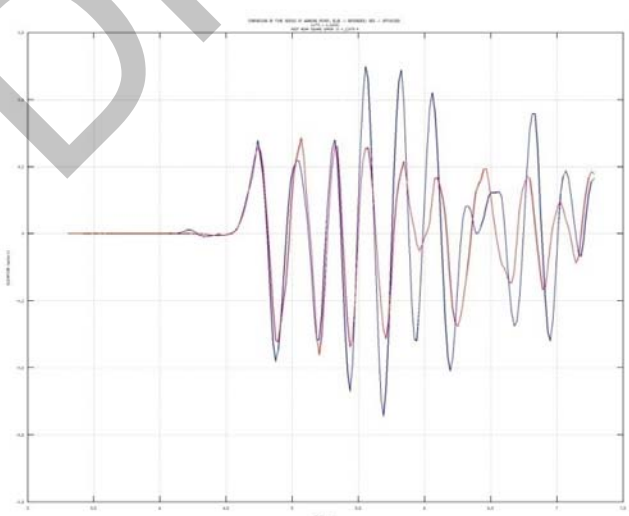

Figure 46 Attempt 3 for T01_1946Unimak_j1_weco.

DRAFT

For Attempt_4 we went back to Attempt_2, but now with a reduced geographical coverage for Grid A, leaving the grid size the same.

Attempt_4: **Grid_A_opt_72s_v2.dat (nrows=186,ncols=135,nodes=25110,** Δt_A = 9.29 s)

Grid_B_opt_8s_v1.dat (nrows=220,ncols=222,nodes=488740, Δt_B = 3.80 s)

Grid_C_opt_2s_v1.dat (nrows=350,ncols=354,nodes=123900, Δt_C = 1.458 s)

Δt used = 0.98, CPU time = 17.63 minutes, RMSE = 0.1524 m

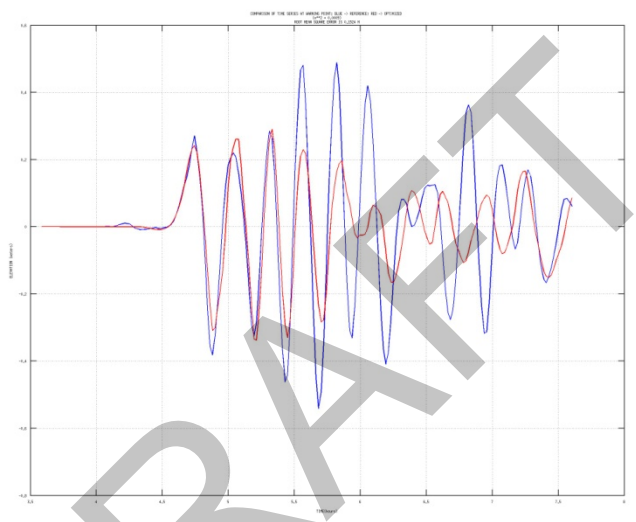

Figure 47 Attempt 4 for T01_1946Unimak_j1_weco.

Attempt_5 uses the same combination as Attempt_1, but with a different Grid C (same as in Attempt_2):

Attempt_5: **Grid_A_opt_72s_v2.dat (nrows=186,ncols=135,nodes=25110,** Δt_A = 9.29 s)

Grid_B_opt_8s_v1.dat (nrows=220,ncols=222,nodes=488740, Δt_B = 3.80 s)

Grid_C_opt_2s_v2.dat (nrows=350,ncols=354,nodes=123900, Δt_C = 1.458 s)

Δt used = 1.4, CPU time = 13.05 minutes, RMSE = 0.163m

DRAFT

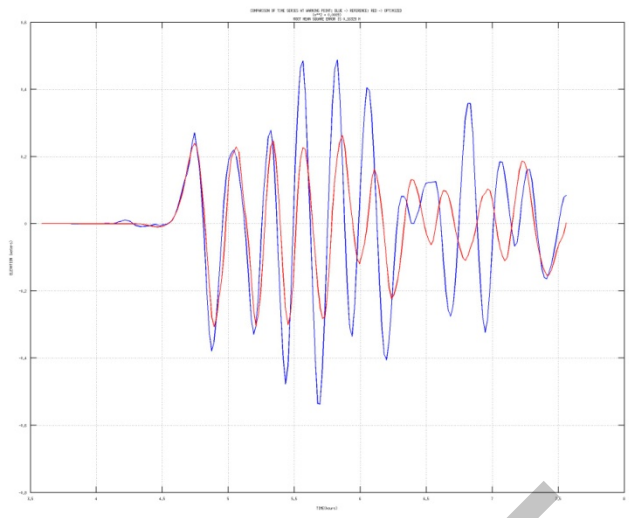

Figure 48 Attempt 5 for T01_1946Unimak_j1_weco.

In this attempt we compared results at a location more to the middle of the entrance (see Figure 49) channel (that is, to the south of the WP, but approximately at the same longitude, locating it more to the middle of the entrance channel in deeper water) to see if the discrepancy in the 4th to 6th waves was an artifact of being so close to the seashore, but it made no difference.

For Attempt_6 we used the same grids as Attempt_1 but with Grid C such that Δx = 2 s, and Δy = 1 s. All of this is in an attempt to see if the 4th peak in the waveform output from the optimal grids increases in amplitude in order to better match the amplitude of the corresponding grid in the reference runs. We do this while trying to maintain the approximate same number of grid nodes. So now we have (see Figure 50)

Attempt_6: **Grid_A_opt_72s_v2.dat (nrows=186,ncols=135,nodes=25110,** Δt_A = 9.29 s)

Grid_B_opt_8s_v1.dat (nrows=220,ncols=222,nodes=488740, Δt_B = 3.80 s)

Grid_C_opt_2&1s_v1.dat (nrows=361,ncols=345,nodes=124545, Δt_C = 1.074 s)

Δt used = 0.97, CPU time = 17.14 minutes, RMSE = 0.135 m

DRAFT

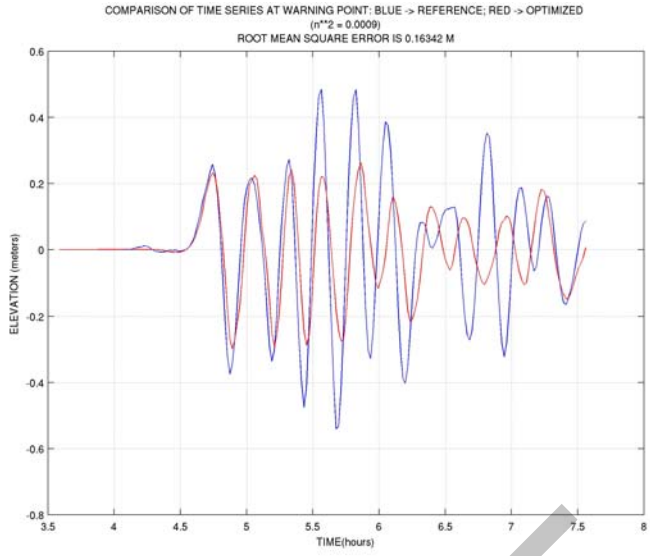

Figure 49 Attempt_5 for T01_1946Unimak_j1_weco with comparison at location more to the middle of the entrance channel.

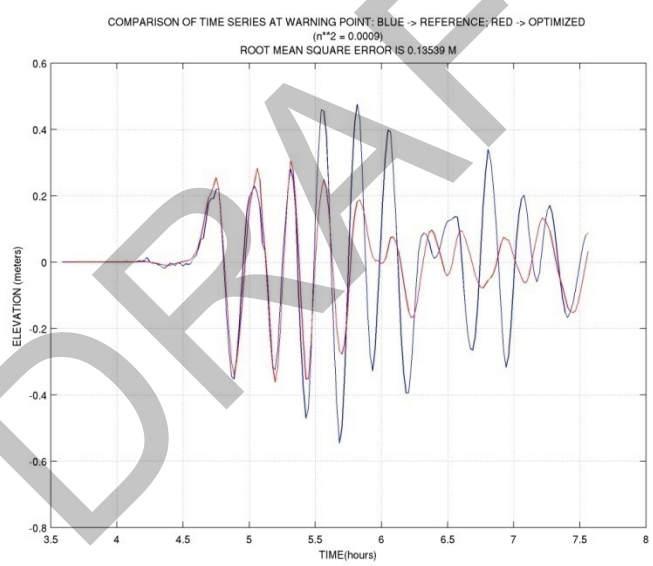

Figure 50 Attempt 6 for T01_1946Unimak_j1_weco.

As in Attempt_5, we tried comparing the time series at a different location, and the result was the same (see Figure 51).

DRAFT

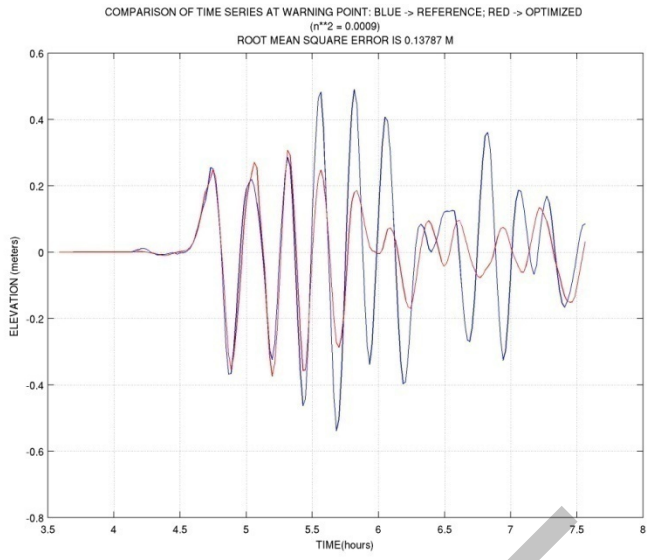

Figure 51 Attempt_6 comparison at location more to the middle of the entrance channel.

Attempt_7 was made with a combination of previously used grids in an attempt to see if the 4th to 6th peaks in the forecast results could be made to match the 4th to 6th peaks in the reference run by using forecast grids A and B, in combination with the reference Grid C (irrespective of CPU time):

Attempt_7: **Grid_A_opt_72s_v2.dat (nrows=186,ncols=135,nodes=25110,** Δt_A = 9.29 s)

Grid_B_opt_8s_v1.dat (nrows=220,ncols=222,nodes=488740, Δt_B = 3.80 s)

Grid_C_ref_2-3rds_v1.dat (nrows=1459,ncols=1686,nodes=2459874, Δt_C = 0.41 s)

Δt used = 0.40, CPU time = 783 minutes, RMSE = 0.117 m

DRAFT

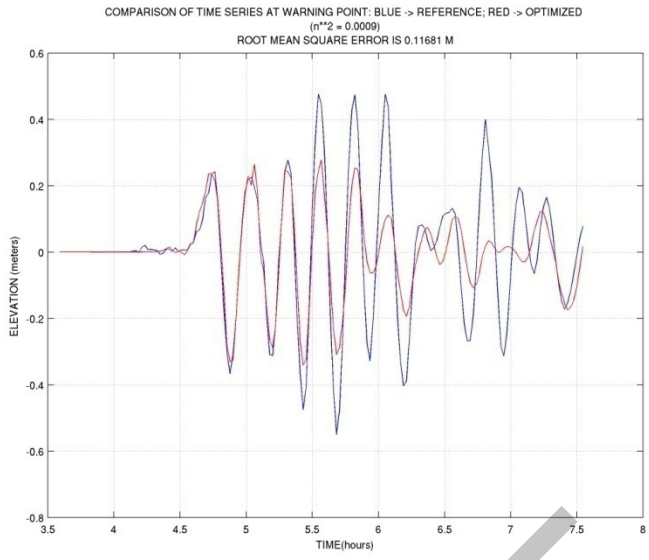

Figure 52 Attempt 7 for T01_1946Unimak_j1_weco.

Here we see that even using the reference Grid C we cannot match the 4th to 6th peaks if we use the forecast grids A and B.

The time series comparison was now tested closer to the entrance of the channel (west of the WP – location 45.56958, -123.95708), but the problem persisted.

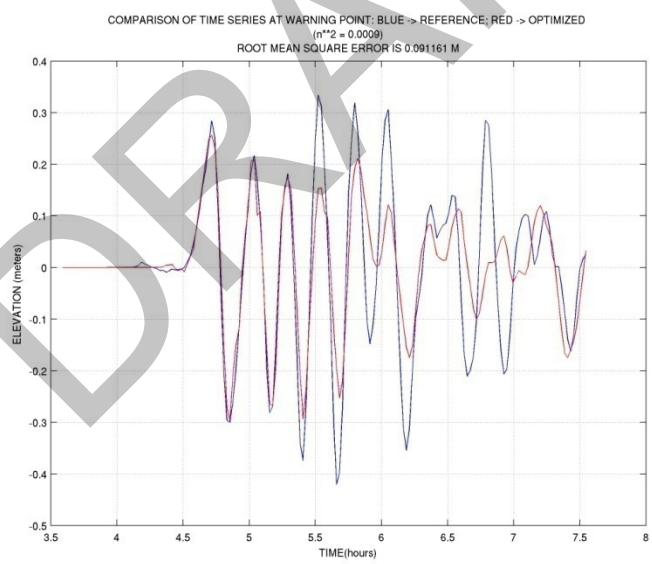

Figure 53 - Location mid-way in the entrance channel.

Next we tried to do the comparison between reference and forecast runs completely outside of the entrance channel and, surprisingly, the problem still persisted. Note that we are using the reference Grid C together with the forecast Grids A and B. Tested location coordinates - 45.56958, -123.95708.

DRAFT

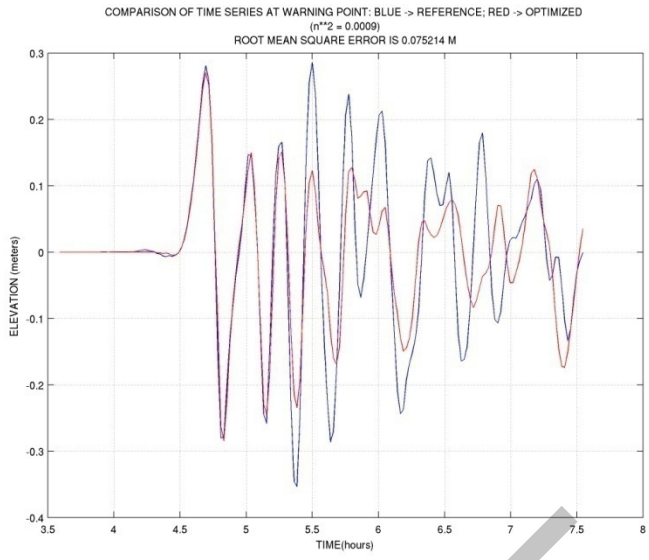

Figure 54 Location completely outside the entrance channel.

In order to try and understand the reasons for discrepancies in the 4th to 6th waves, I tried Attempt_8 with the reference Grid A, forecast Grid B, and reference Grid C.

Attempt_8: **Grid_A_ref_72s_v1.dat (nrows=350,ncols=250,nodes=87500,** Δt_A = 8.01 s)
Grid_B_opt_8s_v1.dat (nrows=220,ncols=222,nodes=488740, Δt_B = 3.80 s)
Grid_C_ref_2-3rds_v1.dat (nrows=361,ncols=345,nodes=124545, Δt_C = 0.41 s)

Δt used = 0.4, CPU time = 803 minutes, RMSE = 0.098 m

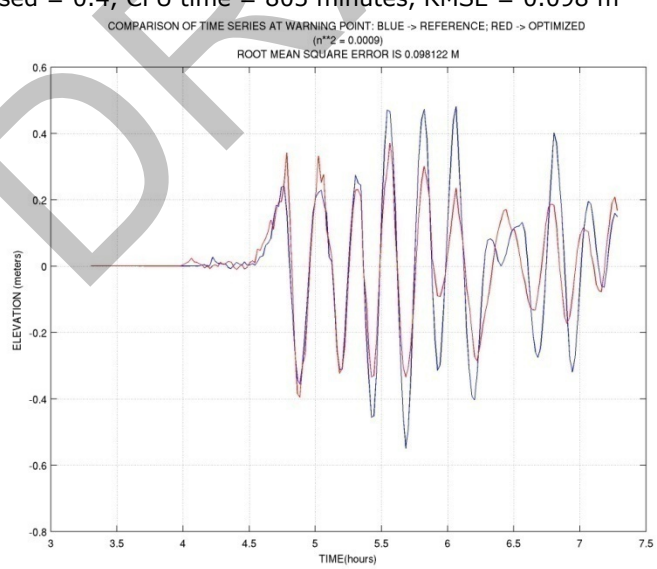

Figure 55 Attempt 8 for T01_1946Unimak_j1_weco.

Though the RMSE decreases, the same problem still persists, though the match is better.

DRAFT

For Attempt_9 use was made, for the first time, of reference Grid B, and the following grid combination was used:

Attempt_9: **Grid_A_opt_72s_v2.dat (nrows=186,ncols=135,nodes=25110,** Δt_A = 9.295 s)
Grid_B_ref_3s_v1.dat (nrows=1021,ncols=961,nodes=981181, Δt_B = 0.97 s)
Grid_C_opt_2&1s_v1.dat (nrows=361,ncols=345,nodes=124545, Δt_C = 1.074 s)

Δt used = 0.96, CPU time = 143 minutes, RMSE = 0.117 m

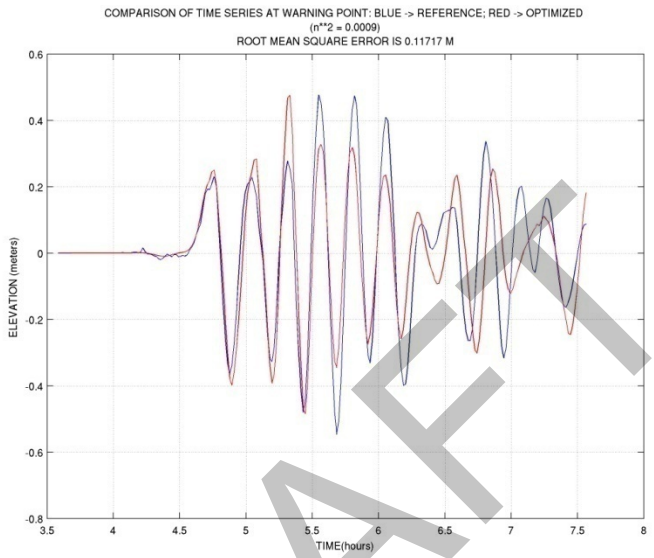

Figure 56 Attempt 9 for T01_1946Unimak_j1_weco.

It is evident that the discrepancy starts with the 3rd peak.

For Attempt_10 we try the same grid combination as Attempt_9 but with a new version for forecast Grid B. For this new version we have reduced the north-south extent of version 1 of forecast Grid B, while at the same time increased its east-west extension. It is called **Grid_B_opt_8s_v2.dat**, with Δt_B = 2.9 s. So now

Attempt_10: **Grid_A_opt_72s_v2.dat (nrows=186,ncols=135,nodes=25110,** Δt_A = 9.295 s)
Grid_B_opt_8s_v2.dat (nrows=161,ncols=266,nodes=42826, Δt_B = 2.9 s)
Grid_C_opt_2&1s_v1.dat (nrows=361,ncols=345,nodes=124545, Δt_C = 1.074 s)

Δt used = 0.98, CPU time = 20.65 minutes, RMSE = 0.134 m

DRAFT

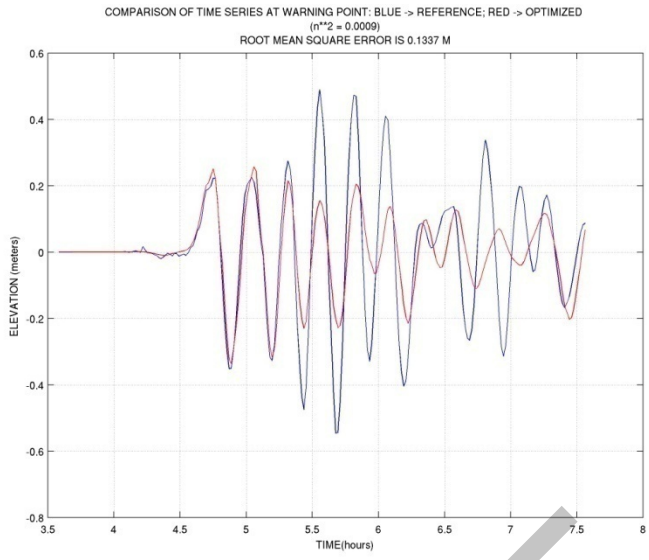

Figure 57 Attempt 10 for T01_1946Unimak_j1_weco.

The comparison outside the entrance channel gives

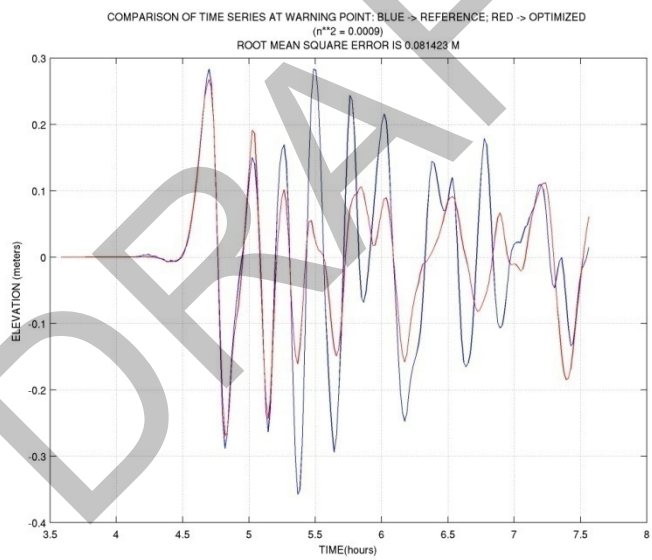

Figure 58 Attempt 10 - Comparison outside of entrance channel.

DRAFT

For Attempt_11 we produced still another version of the forecast Grid B, with Δx = 8s and Δy = 6 s, named **Grid_B_opt_8&6s_v1.dat**, and the following combination of grids (here we used the same combination as for Attempt_2, but with a new version of the forecast Grid B):

Attempt_11:**Grid_A_opt_72s_v1.dat (nrows=383,ncols=289,nodes=110,687,** Δt_A = 8.01 s)
Grid_B_opt_8&6s_v1.dat (nrows=202,ncols=222,nodes=44844, Δt_B = 3.9859 s)
Grid_C_opt_2s_v2.dat (nrows=350,ncols=354,nodes=123900, Δt_C = 1.458 s)

Δt used = 1.4, CPU time = 13.98 minutes, RMSE = 0.1505 m

We can see that the discrepancies have increased still more (see Figure 59). Making the comparison completely outside the entrance channel, we still see discrepancies (see Figure 60).

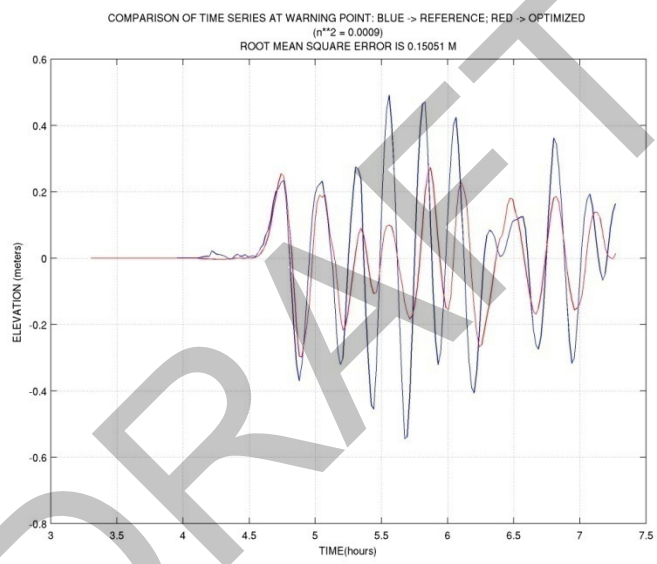

Figure 59 Attempt 11 for T01_1946Unimak_j1_weco.

DRAFT

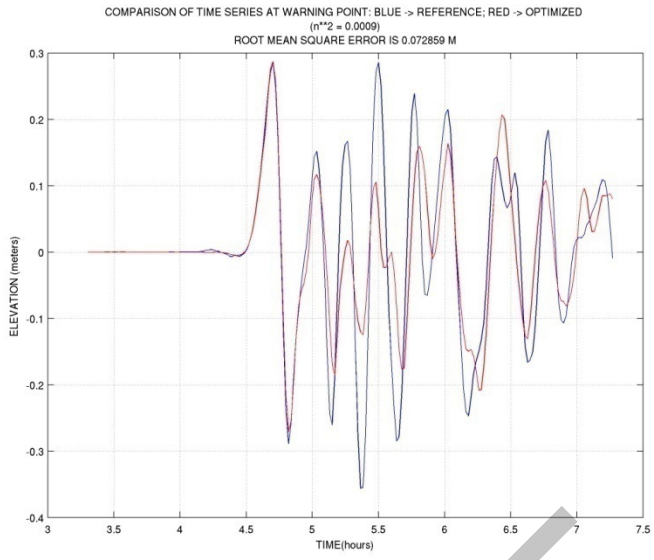

Figure 60 Time series results at a warning point location completely outside entrance channel.

At this point, it looks as if the best option up to now in terms of fit and CPU time is Attempt_5. So we try now the same combination as Attempt_5, but with a new version of forecast Grid B, named **Grid_B_opt_8s_v3.dat**.

Attempt_12: **Grid_A_opt_72s_v2.dat (nrows=186,ncols=135,nodes=25110,** Δt_A = 9.29 s)
Grid_B_opt_8s_v3.dat (nrows=192,ncols=159,nodes=30528, Δt_B = 4.62 s)
Grid_C_opt_2s_v2.dat (nrows=350,ncols=354,nodes=123900, Δt_C = 1.458 s)

Δt used = 1.4, CPU time = 11.81 minutes, RMSE = 0.153 m

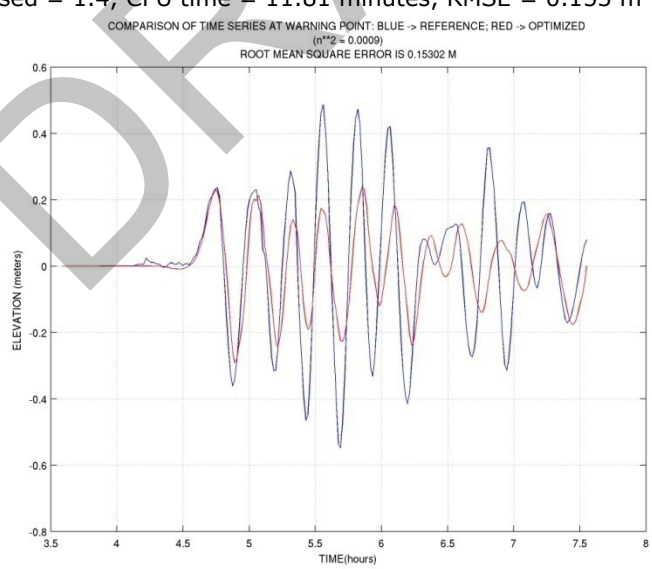

Figure 61 Attempt 12 for T01_1946Unimak_j1_weco.

DRAFT

We now see that this new forecast Grid B has increased the discrepancy in the 3rd peak, and at the same time has not reduced the discrepancy in the 4th to 6th peaks. But CPU time was decreased from 13.05 minutes in Attempt_5 to 11.81 minutes in this attempt.

Looking to decrease CPU time even further, we now try the same as above, but with a new version of forecast Grid C obtained by cropping the Grid C used above both along the top and bottom boundaries. The new grid C was named Grid_C_opt_2s_v3.dat, with Δt_C = 1.4577. Now we have the following combination:

Attempt_13: **Grid_A_opt_72s_v2.dat (nrows=186,ncols=135,nodes=25110,** Δt_A = 9.29 s)
Grid_B_opt_8s_v3.dat (nrows=192,ncols=159,nodes=30528, Δt_B = 4.62 s)
Grid_C_opt_2s_v3.dat (nrows=328,ncols=354,nodes=116112, Δt_C = 1.458 s)

Δt used = 1.4, CPU time = 11.22 minutes, RMSE = 0.153 m

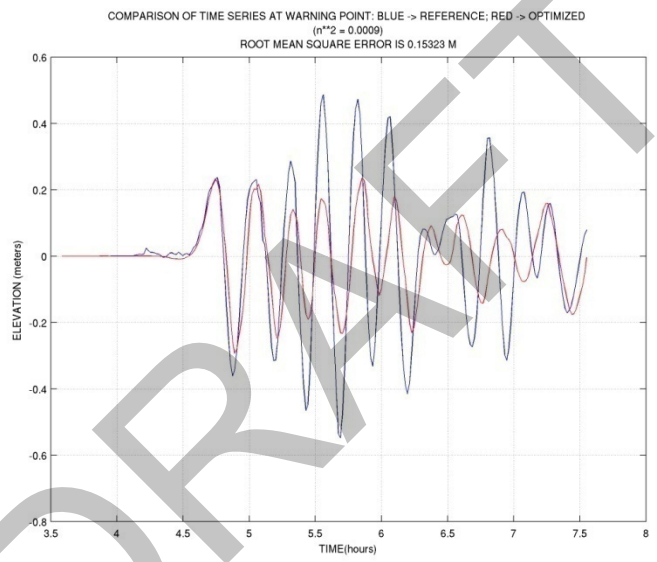

Figure 62 Attempt 13 for T01_1946Unimak_j1_weco.

DRAFT

For Attempt 14 we try the same combination as Attempt_2, but with a changed forecast Grid C, previously created:

Attempt_14: **Grid_A_opt_72s_v1.dat (nrows=383,ncols=289,nodes=110,687,** Δt_A = 8.01 s)
Grid_B_opt_8s_v1.dat (nrows=220,ncols=222,nodes=488740, Δt_B = 3.80 s)
Grid_C_opt_2s_v3.dat (nrows=328,ncols=354,nodes=116112, Δt_C = 1.458 s)

Δt used = 1.4, CPU time = 13.71 minutes, RMSE = 0.135 m

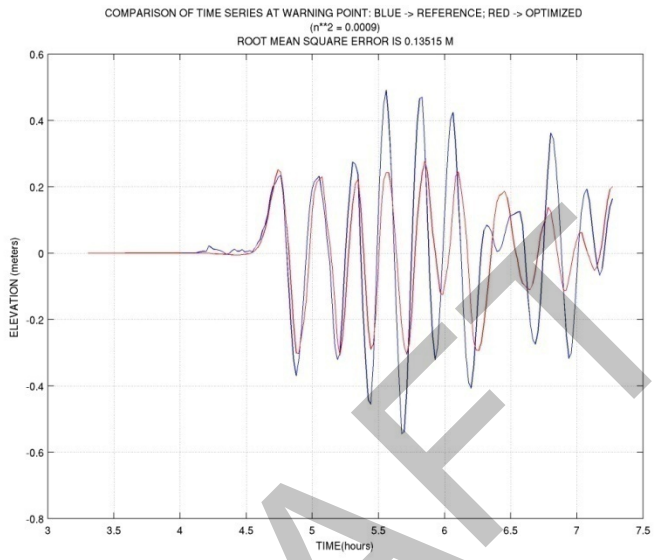

Figure 63 Attempt 14 for T01_1946Unimak_j1_weco.

Still looking for a better match between the reference and forecast 4th to 6th peaks, and a reduced CPU time, we next tried, as Attempt_15, a new version of the forecast Grid C, named **Grid_C_opt_2s_v4.dat**, with Δt_C =1.575.

Attempt_15: **Grid_A_opt_72s_v1.dat (nrows=383,ncols=289,nodes=110,687,** Δt_A = 8.01 s)
Grid_B_opt_8s_v1.dat (nrows=220,ncols=222,nodes=488740, Δt_B = 3.80 s)
Grid_C_opt_2s_v4.dat (nrows=350,ncols=306,nodes=107100, Δt_C = 1.575 s)

Δt used = 1.54, CPU time = 11.6 minutes, RMSE = 0.137 m

DRAFT

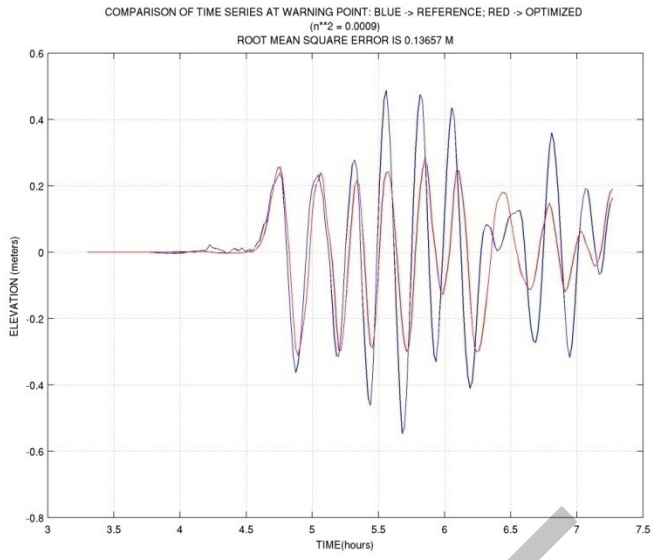

Figure 64 Attempt 15 for T01_1946Unimak_j1_weco.

Seeing no change, we next produce still another version of forecast Grid C, named Grid_C_opt_72s_v4.dat, with ΔtC =1.575.

Attempt_16: **Grid_A_opt_72s_v1.dat (nrows=383,ncols=289,nodes=110,687,** Δt_A = 8.01 s)
Grid_B_opt_8s_v1.dat (nrows=220,ncols=222,nodes=488740, Δt_B = 3.80 s)
Grid_C_opt_2s_v5.dat (nrows=328,ncols=279,nodes=91512, Δt_C = 1.575 s)

Δt used = 1.54, CPU time = 10.85 minutes, RMSE = 0.136 m

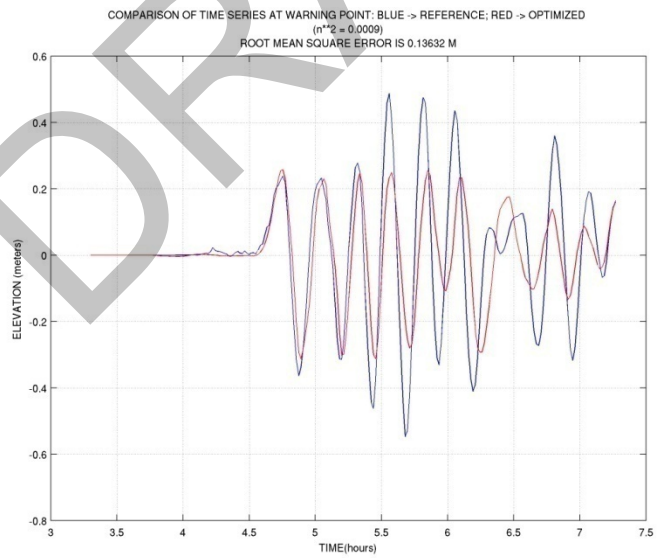

Figure 65 Attempt 16 for T01_1946Unimak_j1_weco

Still no change in the differences between the reference and forecast results.

We next tried still another version of forecast Grid C, named **Grid_C_opt_2s_v6.dat**, with Δt_C =1.651 s.

DRAFT

Attempt_17: **Grid_A_opt_72s_v1.dat (nrows=383,ncols=289,nodes=110,687,** Δt_A = 8.01 s)
Grid_B_opt_8s_v1.dat (nrows=220,ncols=222,nodes=488740, Δt_B = 3.80 s)
Grid_C_opt_2s_v6.dat (nrows=328,ncols=257,nodes=84296, Δt_C = 1.651 s)

Δt used = 1.6, CPU time = 9.82 minutes, RMSE = 0.137 m

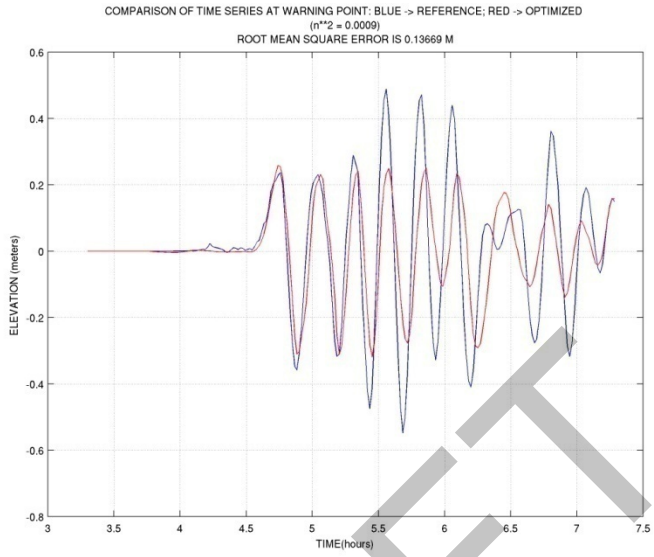

Figure 66 Attempt 17 for T01_1946Unimak_j1_weco.

The best match between reference and forecast results was attained with Attempt_8, with a RMSE = 0.098, but at a cost of 803 minutes in CPU time since two reference grids were used. Amongst the attempts where all grids used were forecast, the best match is obtained for Attempt_1 and Attempt_3, both with RMSE = 0.125 m, but CPU times of 14.22 and 18.67 minutes, respectively. Attempt_17 has a CPU time of 9.82, and a RMSE = 0.137 m. But none could reproduce the amplitudes of the 4th t- 6th peaks in the wave train.

Again, to see whether the increased amplitudes of the 4th to 6th waves in the reference runs was also seen in the waves before entering the entrance channel, Figure 4-24 below shows the time histories taken at the 50 meters isobath outside the channel entrance, located approximately 5.453 km west of the WP. The exact point location is Lat = 45.568796° N, Long = -124.013113° W. Figure 4-25 below shows the time series comparison inside the bay, just south of the city of Garibaldi (Lat = 45.516889° N , Long = -123.914545° W). So we have the situation that at the 50 m isobath the first wave is the highest, and inside the channel and bay it is the 4th and 5th waves that are the highest. And the heights inside the channel and bay are larger. It looks as if the effect we are seeing is a combination of shoaling and a resonance effect. And the resonance effect seems impossible to be recreated with the forecast grid C which, in addition to having 2 s resolution (versus 2/3 s resolution for the forecast grid), does not cover the entire bay (as the forecast grid does). It should be mentioned that this problem was not encountered in all of the synthetic historical tsunamis.

If, as mentioned above, the effect is due to the fact that the forecast grid C does not cover the whole bay as the reference grid C does, another test was done in which the reference grid C was re-gridded to a resolution of 2 s (the same resolution as the forecast grid C), but the area coverage was left as for reference grid C. The results are shown below in Figure 4-26. As can be seen, we still get the result that the 4-6th reference waves still become higher than for the "forecast" results, which seems to

DRAFT

suggest that the mismatch is then due to the lower resolution (2 s) of the forecast grid C versus the reference grid C (2/3 s).

DRAFT

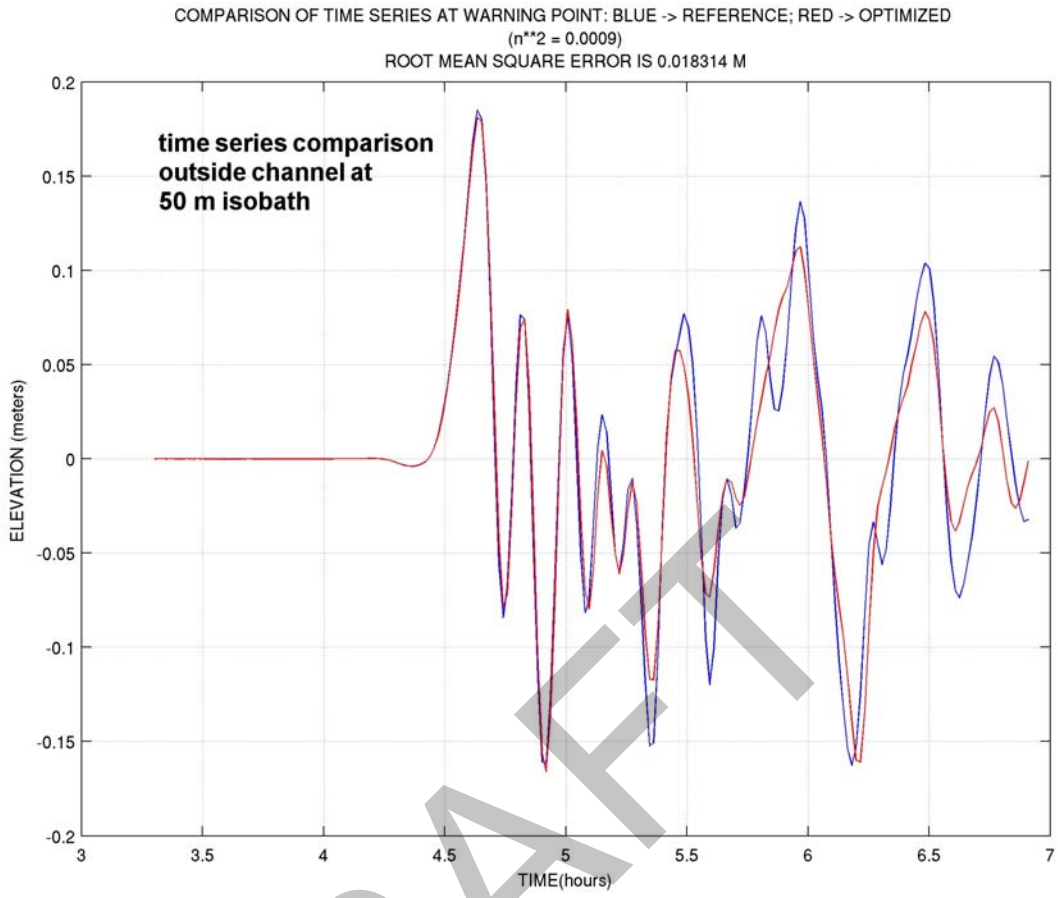

Figure 67 T01_1946Unimak_j1_weco – time history at 50 m isobath west of entrance to the channel.

DRAFT

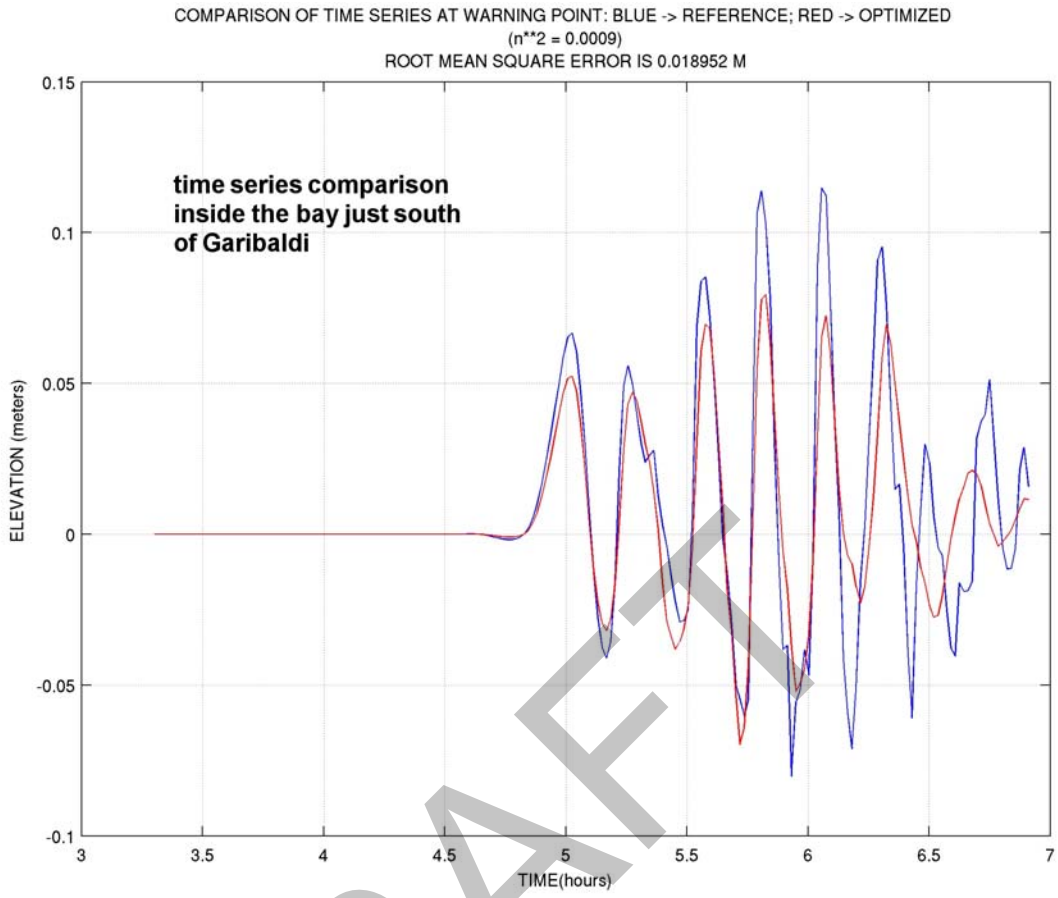

Figure 68 T01_1946Unimak_j1_weco – time history inside bay just south of the city of Garibaldi

DRAFT

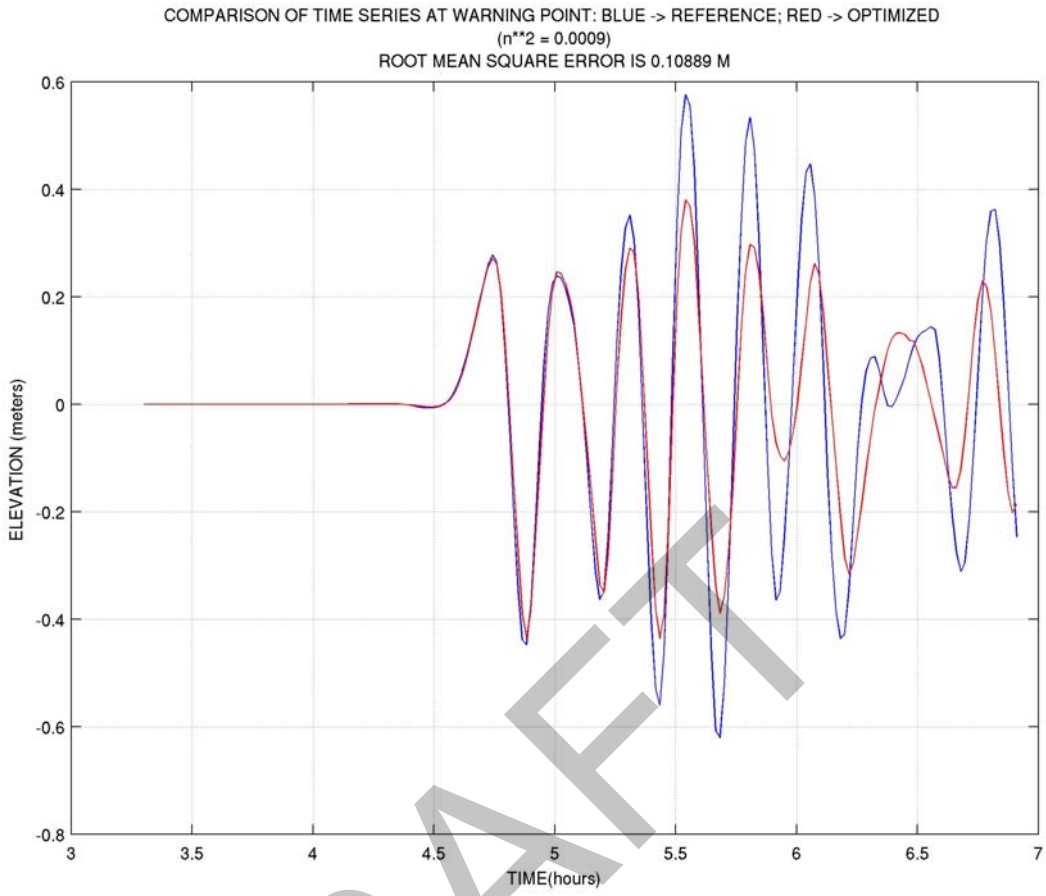

Figure 69 Time history comparison in which the "forecast" grid C has the same area coverage as the reference grid C, but a resolution of 2 s.

DRAFT

Examples of the *.in files used for the reference and forecast grids are:

```
0.001    Minimum amplitude of input offshore wave (m):
1        Input minimum depth for offshore (m)
0.1      Input "dry land" depth for inundation (m)
0.0009   Input friction coefficient (n**2)
1      let a and b run up
30.0   max eta before blow up (m)
0.4      Input time step (sec)
36000    Input amount of steps (4 hrs)
20       Compute "A" arrays every n-th time step, n=
2        Compute "B" arrays every n-th time step, n=
160      Input number of steps between snapshots (62.4 s
0        ...Starting from
1        ...Saving grid every n-th node, n=
Grid_A_ref_72s_v1.dat
Grid_B_ref_3s_v1.dat
Grid_C_ref_2-3rds_v11.dat
/home/amercado/DATA/Pacific_sources/
      /home/amercado/DATA/G1/MOST_runs_2/MOST_output_2/
```

Table 7 Example *.in file for Reference runs

```
0.001    Minimum amplitude of input offshore wave (m):
1        Input minimum depth for offshore (m)
0.1      Input "dry land" depth for inundation (m)
0.0009   Input friction coefficient (n**2)
1      let a and b run up
30.0   max eta before blow up (m)
1.5      Input time step (sec)
9600     Input amount of steps (4 hrs)
5        Compute "A" arrays every n-th time step, n=
2        Compute "B" arrays every n-th time step, n=
40       Input number of steps between snapshots (61.6 s)
0        ...Starting from
1        ...Saving grid every n-th node, n=
Grid_A_opt_72s_v1.dat
Grid_B_opt_8s_v1.dat
Grid_C_opt_2s_v8.dat
/home/amercado/DATA/Pacific_sources/
/home/amercado/DATA/G1/MOST_runs_1/MOST_output_1/
```

Table 8 Example *.in file for forecast runs

DRAFT

5.0 Summary and Conclusions

A set of RIM and forecast model grids have been prepared for Garibaldi, OR. Instabilities were encountered in the preparation of the reference Grid C. These were located in the large surface-piercing large rocks located along the south boundary of the grid, in the rock fronting the entrance channel to the bay, inside the channel, and in the tidal marshes located to the southeast of the bay. They were taken care of by a combination of running bathcorr.f and local smoothing using Surfer.

For some synthetic historical tsunamis after the 3rd wave the RIM tend to produce slightly larger amplitudes than the forecast model. Even after several attempts with different grids, the discrepancy persisted and it looks as if it can only be eliminated by having a higher resolution grid B, but at the expense of CPU time.

Comparison of the only measured tsunami signals at Garibaldi (Tonga 2006 and Kuril 2006) with both the synthetic optimized and reference signals did not produce good results, although results for Tonga 2006 look much better than for Kuril 2006. Both observed signals were extremely weak, on the order of a few centimeters, and extracting the signal from a large tide is not a trivial matter, especially in the presence of outliers in the observed signal.

DRAFT

6.0 Acknowledgements

I would like to acknowledge the valuable help of Dr. Diego Arcas, who recognized the subtle instabilities in the reference Grid C, and who supplied the Matlab program to de-tide the real tsunami signals measured at the Garibaldi tide gauge.

7.0 References

González, F.I., E.N. Bernard, C. Meinig, M.C. Eble, H.O. Mofjeld, and S. Stalin (2005), The NTHMP tsunameter network, *Natural Hazards*, *35*, 25–39.

Titov, V.V., and F.I. González (1997), Implementation and testing of the Method of Splitting Tsunami (MOST) model, *NOAA Tech. Memo. ERL PMEL-112*, 11 pp.

Titov, V.V., F.I. González, E.N. Bernard, M.C., Eble, H.O. Mofjeld, J.C. Newman, and A.J. Venturato (2005), Real-time tsunami forecasting: challenges and solutions, *Natural Hazards*, *35*(1), 41–58.

Titov, V.V., and C.S. Synolakis (1998), Numerical modeling of tidal wave runup. J. Waterw. Port Coast. Ocean Eng., ASCE, 124(4), 157–171.

DRAFT

8.0 Appendix A

8.1 forecast model *.in file for Garibaldi, OR forecast model

0.0001 Minimum amplitude of input offshore wave (m): optimized T01_1946Unimak_j1_weco (4 hrs) Att_17

1 Input minimum depth for offshore (m)

0.1 Input "dry land" depth for inundation (m)

0.0009 Input friction coefficient (n**2)

1 let a and b run up

300.0 max eta before blow up (m)

1.5 Input time step (sec)

9600 Input amount of steps (4 hrs)

5 Compute "A" arrays every n-th time step, n=

2 Compute "B" arrays every n-th time step, n=

40 Input number of steps between snapshots (61.6 s)

0 ...Starting from

1 ...Saving grid every n-th node, n=

DRAFT

8.1 RIM *.in file for Garibaldi, OR forecast model

```
0.001   Minimum amplitude of input offshore wave (m):
1       Input minimum depth for offshore (m)
0.1     Input "dry land" depth for inundation (m)
0.0009  Input friction coefficient (n**2)
1       let a and b run up
30.0    max eta before blow up (m)
0.4     Input time step (sec)
36000   Input amount of steps (4 hrs)
20      Compute "A" arrays every n-th time step, n=
2       Compute "B" arrays every n-th time step, n=
160     Input number of steps between snapshots (62.4 s)
0       ...Starting from
1       ...Saving grid every n-th node, n=
```

DRAFT